

Title Page

Title

Comprehensive Multi-Omics Analysis Identifies HLA-DR and Causal Genes as Critical Factors in Abdominal Aortic Aneurysms Progression

Authors

Xu Guo¹, MSc#; Xiaoxu Zhang¹, MSc#; Tan Li^{2,3}, PhD; Shuai Zhang⁴, MD; Jamol Uzokov⁵, MD PhD; Yuemeng Li⁶, MD; Yu Lun⁷, PhD; Han Jiang⁷, PhD; Chen Chen⁸, PhD MD; Philipp Erhart⁹, MD; Dittmar Böckler⁹, MD; Jian Zhang⁷, PhD MD*; and Yanshuo Han^{1,6}, MD*

Affiliations

1. School of Life and Pharmaceutical Science, Dalian University of Technology, Panjin, China.
2. Department of Cardiovascular Ultrasound, The First Hospital of China Medical University, Shenyang, China.
3. Clinical Medical Research Center of Imaging in Liaoning Province, The First Hospital of China Medical University, Shenyang, China.
4. Department of Endovascular Surgery, The First Affiliated Hospital of Zhengzhou University, Zhengzhou, China.
5. Republican Specialized Scientific Practical Medical Center of Therapy and Medical Rehabilitation, Tashkent, Uzbekistan
6. Department of Vascular Surgery, Central Hospital of Dalian University of Technology, Dalian, China.
7. Department of Vascular Surgery, The First Hospital of China Medical University, Shenyang, China.

8. School of Biomedical Sciences, The University of Queensland, Brisbane, Australia.

9. Department of Vascular and Endovascular Surgery, University of Heidelberg, Heidelberg, Germany.

Corresponding authors at:

Department of Vascular Surgery, the First Hospital of China Medical University, Shenyang, China. No. 155, Nanjingbei Street, Shenyang, China (J. Zhang).

E-mail: jianzhang@cmu.com.cn (J. Zhang)

School of Life and Pharmaceutical Science, Dalian University of Technology, Panjin, China. No. 2, Dagong Road, Panjin, China (Y. Han) E-mail: yanshuohan@dlut.edu.cn (Y. Han).

Contributed equally.

What Is New?

- This study uses a comprehensive multi-omics approach combining single-cell RNA sequencing (scRNA-seq), ATAC-seq, and Mendelian Randomization (MR) analyses to investigate abdominal aortic aneurysms (AAA) pathogenesis.
- Identification of causal genes: The study identifies nine causal genes (e.g., HLA-DRB1, LDAH, SCAPER, NEK9) with roles in AAA progression using genome-wide association study (GWAS) data from AAA patients.
- HLA-DRB1's role in immune response: HLA-DRB1 and other MHC-II molecules are upregulated in myeloid cells, driving immune infiltration and inflammation in AAA.

- Single-cell transcriptomics: The study highlights differential expression of causal genes in distinct cell types, including immune cells such as monocytes, macrophages, and fibroblasts, pinpointing their specific involvement in AAA progression.
- Proteomics validation: Proteomic analysis further supports the findings by showing elevated levels of HLA-DRB1 protein in AAA tissues compared to controls, reinforcing its key role in AAA pathology.
- Cell communication: Enhanced MHC-II pathway activity is identified in myeloid cells, suggesting that aberrant intercellular signaling contributes to the inflammatory microenvironment in AAA.

2. What Are the Clinical Implications?

- Potential therapeutic targets: The identification of HLA-DRB1 and other causal genes provides new potential targets for therapeutic interventions. Targeting these genes, particularly HLA-DRB1, may help modulate the immune response and slow down AAA progression.
- Inflammatory pathways in AAA: The findings emphasize the critical role of the immune system, specifically the MHC-II pathway, in AAA development. Therapeutic strategies aimed at reducing immune cell infiltration and modulating MHC-II signaling in AAA may prove effective.
- Biomarkers for disease progression: Elevated expression of HLA-DRB1, AMH, and SCAPER in myeloid and immune cells in AAA patients suggests their potential use as biomarkers for monitoring disease progression or therapeutic response.
- Personalized treatment approaches: The differential expression of causal

genes in immune cells across patients points toward the feasibility of developing personalized treatment strategies, targeting specific cell types or pathways active in individual patients' AAA pathology.

- Improved risk prediction: The causal relationship established through Mendelian randomization analysis between these genes and AAA risk factors improves our understanding of genetic predisposition, enabling better risk prediction models for AAA.

Abstract

Background: Abdominal aortic aneurysm (AAA) is a complex vascular disease characterized by localized enlargement of the abdominal aorta, with a significant risk of rupture. Understanding the molecular mechanisms underlying AAA development is crucial for identifying potential therapeutic targets. This study integrates multi-omic data, including genome-wide association studies (GWAS), single-cell RNA sequencing (scRNA-seq), and proteomics, to uncover the genetic and molecular contributors to AAA.

Methods: We employed Mendelian Randomization (MR), Summary-data-based Mendelian Randomization (SMR) and Bayesian colocalization analyses to identify causal genes associated with AAA using GWAS data from the FinnGen database. Cis-eQTL and mQTL data from both peripheral blood mononuclear cells (PBMCs) and aortic tissues were integrated. Single-cell RNA sequencing (scRNA-seq) was conducted on AAA tissues and PBMCs to explore gene expression at the cellular level. ATAC-seq data were used to identify regulatory elements, and proteomic analysis was performed to validate the expression of key genes.

Results: We identified nine causal genes significantly associated with AAA, including LDAH, NEK9, CSK, PLEKHJ1, PSRC1, SCAPER, FAM66C, AMH, and HLA-DRB1. Notably, LDAH and NEK9 were associated with reduced AAA risk, while AMH and HLA-DRB1 were linked to increased risk. scRNA-seq revealed distinct expression patterns of these genes in immune cells, particularly within myeloid cells, highlighting the role of immune cell infiltration in AAA pathogenesis. The ATAC-seq analysis showed differential chromatin accessibility in regions associated with these genes, particularly within HLA-DRB1, suggesting its critical role in MHC-II signaling. CellChat analysis highlighted an increased level of communication between myeloid cells via the MHC-II pathway, particularly between macrophages and T cells, further implicating this pathway in AAA pathogenesis. Proteomic validation confirmed the upregulation of HLA-DRB1 in AAA and rupture AAA tissues.

Conclusion: This multi-omic study provides a comprehensive view of the molecular landscape of AAA, identifying key genetic and epigenetic factors involved in its pathogenesis. The upregulation of HLA-DRB1 and the MHC-II signaling pathway in immune cells is a central mechanism driving AAA progression, while the protective roles of LDAH and NEK9 highlight potential therapeutic targets. These findings offer new insights into the molecular basis of AAA and pave the way for precision medicine approaches in its treatment.

Keywords: Abdominal Aortic Aneurysm; Single-cell RNA sequencing; Multi-Omics, Mendelian Randomization; Expression Quantitative Trait Loci; Myeloid Cells; HLA-DRB1.

1. Introduction

Abdominal aortic aneurysm (AAA) is a life-threatening condition characterized by the progressive dilation of the abdominal aorta, which can lead to fatal rupture if left untreated^{1,2}. Despite significant advancements in vascular surgery and imaging techniques, the molecular mechanisms underlying AAA development remain incompletely understood, necessitating further research to identify potential therapeutic targets^{3,4}. Recent advancements in high-throughput genomic technologies have enabled the identification of numerous genetic loci associated with AAA, providing insights into its complex genetic architecture^{5,6}.

Recent years have seen a surge in genomic and multi-omic studies aimed at unraveling the genetic and molecular landscape of AAA. Genome-wide association studies (GWAS) have identified multiple loci associated with AAA, providing a valuable resource for understanding the genetic predisposition to this condition. In the context of AAA, several GWAS have been conducted, revealing novel loci implicated in the disease^{7,8}. However, the biological relevance of these loci and their causal roles in AAA development remain to be fully elucidated. In particular, integrating GWAS data with expression quantitative trait loci (eQTL) and methylation QTL (mQTL) analyses offers a robust framework for identifying causal genes and understanding the regulatory mechanisms that drive disease pathology⁹. Mendelian randomization (MR) serves as a powerful tool within this framework, allowing researchers to infer causal relationships between gene expression and disease risk by leveraging genetic variants as instrumental variables¹⁰.

Furthermore, colocalization analysis can refine these findings by determining whether the genetic variants influencing gene expression and AAA risk are shared, thereby pinpointing potential therapeutic targets¹¹.

Single-cell RNA sequencing (scRNA-seq) has further enriched our understanding of AAA by enabling the detailed characterization of cellular heterogeneity within aneurysmal tissues¹²⁻¹⁴. This technology allows for the identification of cell type-specific gene expression patterns and the dissection of complex tissue environments, providing insights into the cellular contributors to disease progression¹⁵. These technologies enable the detailed characterization of cell-specific gene expression patterns and the identification of key regulatory elements that may contribute to disease progression. Moreover, the integration of these data with Mendelian randomization (MR) analyses can help establish causal relationships between gene expression and AAA risk, further enhancing our understanding of the disease's etiology. Additionally, ATAC-seq (Assay for Transposase-Accessible Chromatin using sequencing) has been employed to map the chromatin accessibility landscape¹⁶, revealing regulatory elements that may play critical roles in modulating gene expression in AAA. Proteomics complements these genomic and transcriptomic approaches by providing a direct measure of protein abundance and modifications, thus offering insights into the functional consequences of genetic and epigenetic alterations. By integrating these multi-omic data layers, researchers can construct a comprehensive view of the molecular networks underlying AAA¹⁷, identify key regulatory pathways, and prioritize candidate genes for further study.

In this study, we employed a comprehensive strategy to identify candidate genes contributing to AAA by integrating GWAS data with expression quantitative trait loci (eQTL) data from peripheral blood mononuclear cells (PBMCs) and aortic tissues. Using the Summary-data-based Mendelian Randomization (SMR) tool, we assessed pleiotropic associations between gene expression levels and AAA risk, followed by Bayesian colocalization analysis¹⁸ to pinpoint genes with shared mutations driving AAA pathogenesis. This approach allowed us to narrow down a list of potential causal genes that warrant further investigation. First, utilize eQTL and mQTL data from both peripheral blood mononuclear cells (PBMCs) and aortic tissues to identify causal genes associated with AAA through Mendelian randomization and Bayesian colocalization analysis. Then, employ single-cell RNA sequencing (scRNA-seq) to map the expression profiles of the identified causal genes within distinct cell populations in AAA tissues, thereby elucidating the cellular contributors to AAA pathogenesis. Moreover, use ATAC-seq to identify regulatory elements linked to the identified causal genes and determine their potential roles in gene expression regulation within AAA tissues. And perform proteomic analyses to validate the expression and functional relevance of the identified genes, focusing on the interaction between key signaling pathways and protein abundance in AAA. Finally, to validate the expression and functional relevance of the identified causal genes and pathways through proteomic analysis, immunofluorescence, and other molecular techniques, aiming to confirm their roles in AAA pathogenesis. Explore the involvement of the MHC-II signaling pathway, particularly the gene HLA-DRB1, in mediating

immune responses within AAA tissues, and assess its potential as a therapeutic target.

2. Methods

Detailed descriptions and sources of reagents can be found in the **Supplementary File- Methods**. This study was performed according to the Guidelines of the World Medical Association Declaration of Helsinki and was approved by the local ethics committee of The First Hospital of China Medical University. Firstly, for scRNA-seq part, ethical approval for the study was obtained from the Ethics Committee of The First Hospital of China Medical University (ethical approval number: [2021]134). Furthermore, for proteomics, ATAC-seq, and experimental verification part, AAA patients registered in China Medical University aneurysm Biobank (CMUaB) were analyzed as described previously^{19,20}. Written informed consent was obtained from all participants prior to their inclusion in the study. This process ensured that all subjects were fully informed about the nature, purpose, and potential risks of the study, in accordance with ethical standards and the Declaration of Helsinki.

3. Results

3.1 Identification of Causal Genes for Abdominal Aortic Aneurysm through Colocalization and Mendelian Randomization

The flow chart of the current research was shown in **Figure 1**. To identify candidate effect genes associated with abdominal aortic aneurysm (AAA), we

employed the Summary-data-based Mendelian Randomization (SMR) tool to assess the pleiotropic associations between gene expression levels and AAA.

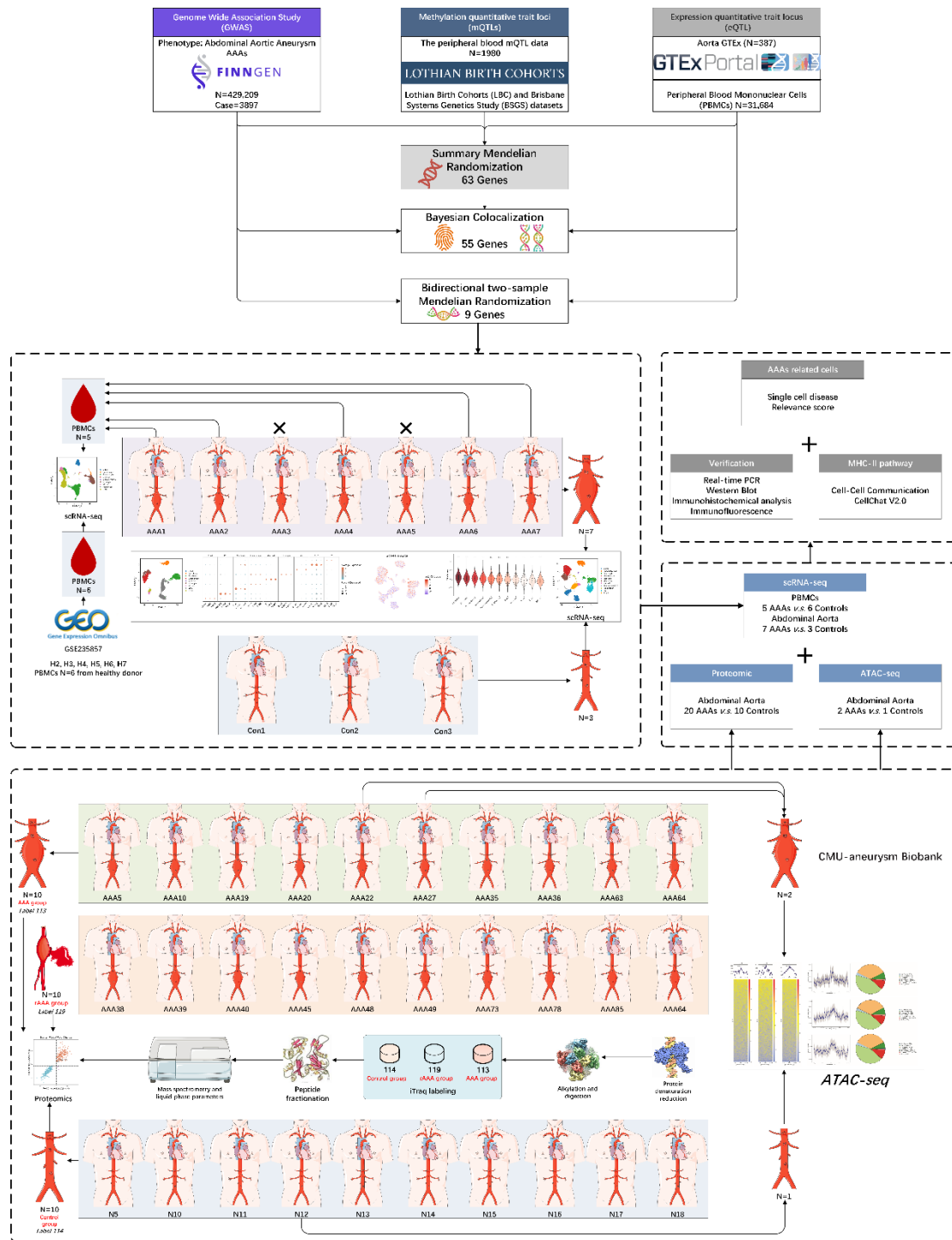


Figure 1. Flowchart of the overall experimental design.

We analyzed AAA genome-wide association study (GWAS) data from the

FinnGen database (**Figure 2A**) alongside cis-eQTL data from PBMCs sourced from eQTLGen, as well as cis-eQTL data from the aorta and methylation quantitative trait loci (mQTL) data from whole blood. The results of these SMR analyses are detailed in **Supplementary File – Excel 1**. Through SMR, we obtained a comprehensive overview of the association levels between all gene regions and AAA, enabling us to identify high-value effect loci. Subsequently, we extracted genes with significant associations from the three analyses (with SMR P-values < 0.05 and GWAS P-values $< 5.0 \times 10^{-4}$) and performed Bayesian colocalization analysis on single nucleotide polymorphisms (SNPs) within ± 100 kb of these genes in relation to AAA GWAS results. This analysis was conducted using eQTL data from both aorta and PBMCs. Genes with colocalization posterior probabilities (coloc.abf-PPH4) greater than 0.75 were considered to share the same mutations associated with AAA, and the results are presented in **Supplementary File – Excel 2**.

We then selected 55 genes that successfully colocalized in either PBMCs or aorta for Mendelian Randomization (MR) analysis in conjunction with AAA GWAS data. Ten genes were excluded due to the absence of valid instrumental variables, leaving 45 genes whose expression was strongly correlated with SNPs (P-value $< 5.0 \times 10^{-8}$) included in the analysis. Prior to executing the MR, we searched the GWAS Catalog (<https://www.ebi.ac.uk/gwas>) for instrumental SNPs linked to these genes to exclude any SNPs associated with AAA outcomes, with search results detailed in **Supplementary File – Excel 3**. No SNPs associated with AAA were found in the PBMC eQTL data. The detailed MR results for all genes are shown in

Figure S1A and **Table 1**. We identified 20 genes in PBMCs that exhibited significant causal effects (P -value < 0.05), including six risk genes: AMH, CESLR2, RAI14, HLA-DRB1, GDF7, and PLAU (**Figure 2B** and **Figure S1B**). A reverse MR causal testing was performed on these 20 effect genes, incorporating SNPs strongly associated with GWAS (P -value $< 5.0 \times 10^{-8}$). The results, illustrated in **Figure 2C**, led to the exclusion of 11 genes due to significant reverse causal effects associated with AAA. Ultimately, we identified nine genes that exert causal effects on AAA, with their odds ratios (OR) and MR test results presented in **Figures 2D, 2E**. Notably, the expression of LDAH, NEK9, CSK, PLEKHJ1, PSRC1, SCAPER, and FAM66C was associated with a reduced risk of AAA, with LDAH demonstrating the highest number of instrumental SNPs and the most significant causal effect ($P = 3.4 \times 10^{-9}$). Conversely, increased expression of AMH and HLA-DRB1 was associated with an elevated risk of AAA, with OR values of 1.1845 and 1.2455, respectively, highlighting their potential as drug targets. All nine genes showed no abnormalities in pleiotropy tests, heterogeneity tests, direction tests, and Steiger tests, as detailed in **Supplementary File – Excel 4**.

Table 1. MR results of PBMC eQTL for colocalized genes with AAA GWAS.

Exposure	Outcome	Exposure	Method	Number of SNPs	Effect estimate	Standard error	P value	Proportion of Variance Explained
eqtl-a-ENSG0000011028	AAA	MRC2	Inverse variance weighted	2	0.09154	0.195156	0.639027	0.004267
eqtl-a-ENSG0000039560	AAA	RAI14	Inverse variance weighted	3	0.213725	0.096284	0.026438	0.017113
eqtl-a-ENSG0000065000	AAA	AP3D1	Wald ratio	1	0.130206	0.079761	0.102585	0.024519
eqtl-a-ENSG0000087157	AAA	PGS1	Inverse variance weighted	3	-0.0747	0.20476	0.715244	0.012112
eqtl-a-ENSG0000087237	AAA	CETP	Inverse variance weighted	5	0.141194	0.123828	0.254187	0.026973
eqtl-a-ENSG0000089818	AAA	NECAP1	Inverse variance weighted	3	-0.12203	0.048334	0.011577	0.060203
eqtl-a-ENSG0000100285	AAA	NEFH	Inverse variance weighted	3	-0.03517	0.054552	0.519108	0.041125
eqtl-a-ENSG0000103653	AAA	CSK	Inverse variance weighted	3	-0.1144	0.052002	0.027813	0.048017
eqtl-a-ENSG0000104885	AAA	DOT1L	Wald ratio	1	-1.05965	0.259721	4.50E-05	0.005244
eqtl-a-ENSG0000104886	AAA	PLEKHJ1	Wald ratio	1	-0.38382	0.090402	2.18E-05	0.016915
eqtl-a-ENSG0000104899	AAA	AMH	Wald ratio	1	0.169283	0.067386	0.012	0.032134
eqtl-a-ENSG0000118961	AAA	LDAH	Inverse variance weighted	5	-0.23401	0.039598	3.43E-09	0.08665
eqtl-a-ENSG0000119638	AAA	NEK9	Wald ratio	1	-0.64459	0.291296	0.026908	0.001677
eqtl-a-ENSG0000119640	AAA	ACYP1	Wald ratio	1	-0.54918	0.171692	0.001381	0.004207
eqtl-a-ENSG0000119684	AAA	MLH3	Inverse variance weighted	5	-0.1202	0.047984	0.012242	0.060355
eqtl-a-ENSG0000119718	AAA	EIF2B2	Inverse variance weighted	3	-0.08352	0.046964	0.075343	0.078164
eqtl-a-ENSG0000122861	AAA	PLAU	Inverse variance weighted	3	0.288425	0.065178	9.63E-06	0.02789
eqtl-a-ENSG0000123329	AAA	ARHGAP9	Inverse variance weighted	2	-0.04232	0.050875	0.405485	0.058655
eqtl-a-ENSG0000123384	AAA	LRP1	Inverse	3	-0.16376	0.177098	0.355116	0.004002

			variance weighted					
eqtl-a-ENSG00000134222	AAA	PSRC1	Inverse variance weighted	3	-0.16594	0.043826	0.000153	0.062531
eqtl-a-ENSG00000136381	AAA	IREB2	Inverse variance weighted	4	-0.13414	0.059046	0.023099	0.080353
eqtl-a-ENSG00000140386	AAA	SCAPER	Inverse variance weighted	4	-0.13592	0.037885	0.000334	0.099474
eqtl-a-ENSG00000140836	AAA	ZFHX3	Inverse variance weighted	4	-0.17276	0.094942	0.068818	0.018664
eqtl-a-ENSG00000143126	AAA	CELSR2	Wald ratio	1	0.148599	0.075741	0.049769	0.022306
eqtl-a-ENSG00000143869	AAA	GDF7	Wald ratio	1	0.418075	0.152078	0.005976	0.007496
eqtl-a-ENSG00000147324	AAA	MFHAS1	Inverse variance weighted	3	0.220724	0.11453	0.053952	0.031168
eqtl-a-ENSG00000154319	AAA	FAM167A	Inverse variance weighted	4	0.116021	0.086785	0.181263	0.072454
eqtl-a-ENSG00000162650	AAA	ATXN7L2	Wald ratio	1	0.026268	0.20172	0.896391	0.006902
eqtl-a-ENSG00000164024	AAA	METAP1	Inverse variance weighted	2	-0.75026	0.240869	0.001841	0.004049
eqtl-a-ENSG00000164867	AAA	NOS3	Wald ratio	1	0.120219	0.071463	0.09252	0.021936
eqtl-a-ENSG00000166311	AAA	SMPD1	Inverse variance weighted	2	0.082312	0.180137	0.647712	0.004772
eqtl-a-ENSG00000171044	AAA	XKR6	Wald ratio	1	-0.25971	0.1008	0.009982	0.013452
eqtl-a-ENSG00000175600	AAA	SUGCT	Wald ratio	1	-0.26336	0.201912	0.192118	0.007093
eqtl-a-ENSG00000179344	AAA	HLA-DQB1	Inverse variance weighted	3	-0.00973	0.057587	0.865812	0.199125
eqtl-a-ENSG00000196126	AAA	HLA-DRB1	Wald ratio	1	0.219541	0.105466	0.037377	0.349073
eqtl-a-ENSG00000196735	AAA	HLA-DQA1	Inverse variance weighted	5	-0.00549	0.072134	0.939305	0.398974
eqtl-a-ENSG00000198208	AAA	RPS6KL1	Wald ratio	1	-0.15938	0.081624	0.050871	0.021284
eqtl-a-ENSG00000198502	AAA	HLA-DRB5	Inverse variance weighted	8	0.03907	0.057262	0.495054	0.21224
eqtl-a-ENSG00000204516	AAA	MICB	Inverse variance weighted	3	0.017625	0.054337	0.745665	0.176255
eqtl-a-ENSG00000223534	AAA	HLA-DQB1-AS1	Inverse variance weighted	3	0.068285	0.065457	0.296855	0.528143
eqtl-a-ENSG00000226711	AAA	FAM66C	Wald ratio	1	-0.53214	0.133446	6.67E-05	0.107264
eqtl-a-ENSG00000240053	AAA	LY6G5B	Inverse variance weighted	2	0.017431	0.064113	0.785713	0.091268
eqtl-a-ENSG00000246090	AAA	LOC100507053	Inverse variance	4	0.008198	0.102282	0.93612	0.128609

			weighted				
--	--	--	----------	--	--	--	--

Additionally, we conducted MR analysis using aorta eQTL data in conjunction with AAA GWAS. Due to the limited sample size of the aorta eQTL dataset (only 387 samples) and the lack of effect allele frequency data for non-significant SNPs (precluding effective reverse MR causal testing), these MR results are considered supplementary to the previous analysis. During the confounding factor adjustment process, rs11172113 was identified as having a causal effect on abdominal aortic aneurysm and was subsequently removed (**Supplementary File – Excel 3**). A total of 33 genes with suitable instrumental variables from the eQTL data were included in the MR analysis, with results provided in **Table 2** and **Figure S2A**. Scatter plot of MR test results for the 23 genes with $P < 0.05$ (**Figure S2B-X**). Among the nine genes validated in PBMCs, low-risk genes LDAH and SCAPER, as well as high-risk genes AMH and HLA-DRB1, were also confirmed in the aorta. However, the causal effects of FAM66C and NEK9 in the aorta were found to be opposite to those observed in PBMCs, indicating that increased expression may elevate AAA risk. Further evidence is needed to validate the effect direction of FAM66C and NEK9. Results from pleiotropy tests, heterogeneity tests, direction tests, and Steiger tests are presented in **Supplementary File – Excel 5**.

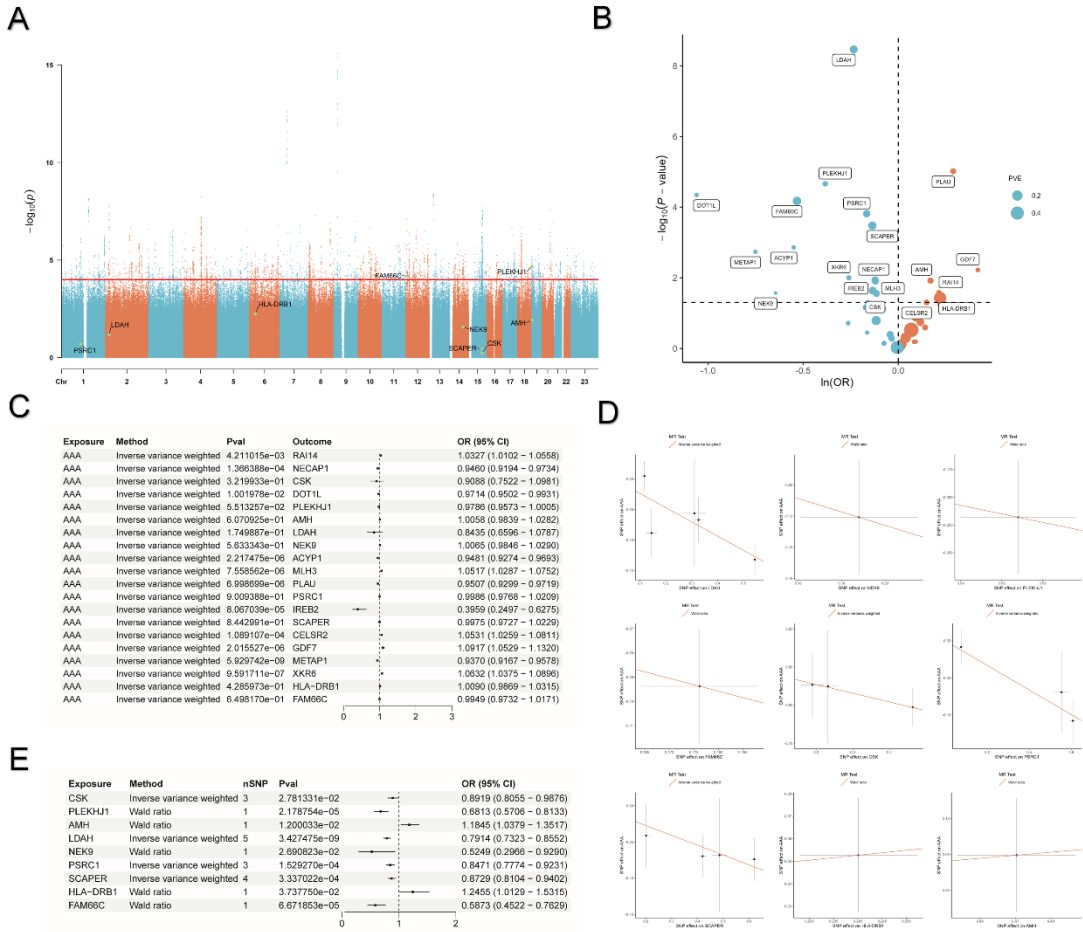


Figure 2. Genetic Analysis and Mendelian Randomization Results for Causal Genes in GWAS of Abdominal Aortic Aneurysm. (A) Manhattan plot of the AAA GWAS. The labels indicate the locations of the 9 causal genes identified in this study, with the y-axis representing the negative log of the p-value for one of the instrumental SNPs. (B) MR analysis results of colocalized genes. The teal points on the left side of the volcano plot represent genes with a negative OR, while the orange-red points on the right side indicate genes with an OR greater than zero. The y-axis shows the negative logarithm of the p-value, and the size of the points represents the proportion of variance explained (PVE). (C) Forest plot of reverse MR analysis results. (D) Forest plot of the 9 causal genes. (E) MR scatter plot for the 9 causal genes. In

cases where the number of instrumental SNPs is greater than 1, inverse variance weighted regression is used, and where the number is equal to 1, the Wald ratio estimate is applied.

Table 2. MR results of Aorta eQTL for colocalized genes with AAA GWAS.

Exposure	Outcome	Exposure	Method	Number of SNPs	Effect estimate	Standard error	P value	Proportion of Variance Explained
ENSG0000011028	AAA	MRC2	Wald ratio	1	0.203053	0.08499	0.016888	0.151767
ENSG0000039560	AAA	RAI14	Wald ratio	1	0.156931	0.118561	0.185629	0.075985
ENSG0000065000	AAA	AP3D1	Wald ratio	1	-0.24259	0.142257	0.088142	0.093947
ENSG0000087157	AAA	PGS1	Wald ratio	1	-0.0143	0.11095	0.897456	0.075324
ENSG0000089818	AAA	NECAP1	Wald ratio	1	0.093583	0.036397	0.010136	0.487764
ENSG0000104899	AAA	AMH	Inverse variance weighted	2	0.112148	0.040752	0.005924	0.406561
ENSG0000118961	AAA	LDAH	Inverse variance weighted	2	-0.19234	0.032483	3.20E-09	0.494331
ENSG0000119638	AAA	NEK9	Inverse variance weighted	2	0.250653	0.110495	0.023301	0.272526
ENSG0000119718	AAA	EIF2B2	Inverse variance weighted	3	-0.21285	0.046498	4.70E-06	0.514105
ENSG0000134222	AAA	PSRC1	Wald ratio	1	-0.04322	0.069246	0.53252	0.189773
ENSG0000140386	AAA	SCAPER	Inverse variance weighted	2	-0.28903	0.053317	5.93E-08	0.477019
ENSG0000143028	AAA	SYPL2	Wald ratio	1	0.20649	0.046066	7.38E-06	0.433724
ENSG0000143126	AAA	CELSR2	Wald ratio	1	0.171606	0.088457	0.052379	0.163802
ENSG0000143869	AAA	GDF7	Inverse variance weighted	2	-0.41756	0.102253	4.43E-05	0.182471
ENSG0000162650	AAA	ATXN7L2	Inverse variance weighted	2	0.091637	0.333391	0.78342	0.165196
ENSG0000164024	AAA	METAP1	Wald ratio	1	-0.03542	0.076166	0.641903	0.239322

ENSG00000172955	AAA	ADH6	Wald ratio	1	0.211484	0.066311	0.001426	0.120389
ENSG00000175600	AAA	SUGCT	Inverse variance weighted	2	-0.52967	0.054576	2.86E-22	0.394547
ENSG00000179344	AAA	HLA-DQB1	Inverse variance weighted	4	0.090943	0.019601	3.49E-06	1.364153
ENSG00000187758	AAA	ADH1A	Wald ratio	1	0.185677	0.049304	0.000166	0.205269
ENSG00000196126	AAA	HLA-DRB1	Wald ratio	1	0.162558	0.069854	0.019958	0.22132
ENSG00000196616	AAA	ADH1B	Wald ratio	1	0.462576	0.122285	0.000155	0.077159
ENSG00000196735	AAA	HLA-DQA1	Inverse variance weighted	3	0.148835	0.035672	3.01E-05	0.55073
ENSG00000198099	AAA	ADH4	Wald ratio	1	-0.0988	0.056492	0.080292	0.205812
ENSG00000198208	AAA	RPS6KL1	Wald ratio	1	-0.15158	0.101608	0.135746	0.079732
ENSG00000198502	AAA	HLA-DRB5	Inverse variance weighted	3	0.07954	0.025988	0.002209	0.855504
ENSG00000204516	AAA	MICB	Wald ratio	1	0.075347	0.030292	0.012871	0.415491
ENSG00000223534	AAA	HLA-DQB1-AS1	Inverse variance weighted	4	0.132385	0.02866	3.85E-06	0.775063
ENSG00000224017	AAA	LINC01449	Inverse variance weighted	2	-0.61689	0.063547	2.80E-22	0.20075
ENSG00000226711	AAA	FAM66C	Wald ratio	1	0.212771	0.057206	0.0002	0.200166
ENSG00000240053	AAA	LY6G5B	Wald ratio	1	0.027743	0.077403	0.720031	0.244217
ENSG00000246090	AAA	LOC100507053	Wald ratio	1	0.235536	0.073852	0.001426	0.098785
ENSG00000259422	AAA	LOC101929439	Inverse variance weighted	2	0.156651	0.06071	0.009871	0.270704

3.2 Single-Cell Transcriptomics Reveals the Expression Profile of Causal Genes

To explore the cellular localization of causal genes, we collected samples from seven abdominal aortic aneurysm (AAA) tissues and five peripheral blood mononuclear cell (PBMC) samples. The baseline of participants was shown in

the **Table 1**, resulting in a total of 38,420 aortic tissue cells and 48,184 PBMCs included in the study. Additionally, five healthy aortic tissue samples and six healthy PBMC samples from the GSE235857 dataset were utilized as controls

Supplementary File - Table S1. Figures 3A and Figure 3B present UMAP plots illustrating the two-dimensional projections of single-cell data from AAA PBMCs and aortic tissues, respectively, with cell types annotated. The markers used for cell annotation are displayed in dot plots in **Figures 3C and 3D**. Correspondingly, UMAP plots and cell annotation dot plots for the normal samples are presented in **Figure S3A** and **Figure S3B**.

Table 3. The baseline data of AAA patients (n=7) and normal control group (n=3) included in this study for scRNA-seq.

Variable	AAA1	AAA2	AAA3	AAA4	AAA5	AAA6	AAA7	Control1	Control2	Control3
Age, Yrs	66	72	55	53	63	62	67	59	62	55
Gender	Male	Male	Female	Male	Male	Male	Male	Male	Male	Male
Maximum aneurysmal diameter, mm	92	101	55	56	55	55	95	NA	NA	NA
Rupture	Yes	Yes	No	No	No	No	Yes	NA	NA	NA
Diabetes mellitus	No	No	No	No	No	No	No	No	No	No
Hypertension	Yes	No	No	No	Yes	Yes	Yes	No	Yes	No
Carotid disease	No	No	No	No	No	No	No	No	No	No
Cardiac disease	No	Yes	No	No	Yes	No	No	No	No	No
Renal disease	No	No	No	No	No	No	No	Yes	No	No
Hyperlipidemia	No	No	No	No	No	No	No	Yes	No	No
Stroke	No	Yes	No	No	No	Yes	No	No	No	No
Smoking History	Current	Current	Never	Current	Current	Never	Current	Never	Never	Current
Sample	Tissue +	Tissue +	Tissue	Tissue +	Tissue	Tissue +	Tissue +	-	-	-

	PBMCs	PBMCs		PBMCs		PBMCs	PBMCs			
--	-------	-------	--	-------	--	-------	-------	--	--	--

In the AAA cohort, the top 10 differentially expressed genes are shown in **Figures 3E** and **Figure 3F**. Notably, genes from the HLA family, including HLA-DRB1, were significantly enriched in B cells, dendritic cells (DCs), and monocytes in the PBMCs of AAA patients, whereas these genes exhibited markedly higher expression only in B cells in the control group (**Figure S3G**). In the healthy control aorta cohort, the top 10 differentially expressed genes are shown in **Figures S3C** and **Figure S3D**. The cellular composition of different AAA samples is illustrated in **Figures 3G** and **Figure 3H**, while the proportional bar charts for the control group can be found in **Figures S3E** and **Figure S3F**. In aortic tissues, the proportion of immune cells, including T cells, B cells, and myeloid cells, was significantly higher in the AAA group compared to the control group, indicating immune cell infiltration. Additionally, the marked increase in granulocyte proportion in the PBMCs of AAA patients corroborates the presence of severe inflammation.

To further investigate the association levels between different cell types and AAA, we calculated the association scores for each cell in the AAA single-cell dataset using scDRS, visualizing the results in **Figure S4**. **Figures S4A** and **Figure S4B** demonstrate the cell-disease association levels in AAA aortic tissues, revealing that higher scDRS scores are significantly associated with fibroblasts, monocytes, endothelial cells, and macrophages (in decreasing order of association). In PBMCs, various myeloid cells, including monocytes,

DCs, megakaryocytes, and granulocytes, were also significantly associated with AAA (in decreasing order of association). The application of scDRS highlights the critical role of myeloid immune cells in AAA, providing valuable prior information for subsequent analyses (**Figure S4C** and **Figure S4D**).

Figures 3I and **Figure 3J** present density plots showing the distribution of the expression of nine genes in aortic tissues and PBMCs. We focused on the expression density in fibroblasts, endothelial cells, and myeloid cells, as these cell types are strongly associated with AAA. In the aorta, cells expressing AMH and PSRC1 were rare and thus not discussed further. Notably, NEK9 was distributed in fibroblasts, while NEK9, SCAPER, and HLA-DRB1 exhibited substantial expression in endothelial cells. Concentrated expression regions for HLA-DRB1, CSK, and PLEKHJ1 were identified in myeloid cells. Conversely, in the control group, LDAH and NEK9 were significantly enriched in myeloid cells (**Figure S3G** and **Figure S3H**), while PLEKHJ1 was concentrated in endothelial cells. In PBMCs, significant expression of CSK, PLEKHJ1, NEK9, PSRC1, SCAPER, and HLA-DRB1 was observed in monocytes; CSK was also broadly expressed in granulocytes. In the control group, only NEK9 and PSRC1 were found in myeloid cells (**Figure S3G** and **Figure S3H**). **Figures 3K** and **Figure 3L** describe the overall expression levels of the nine genes in aortic tissues and PBMCs, while Volcano Plot illustrates the differentially expressed genes with indicating differential expression in PBMCs and differential expression in aortic tissues (**Figure 3M**). Three genes, HLA-DRB1, SCAPER, and NEK9, exhibited differential expression in both aortic tissues and PBMCs; however, NEK9 showed contrasting expression levels (highly expressed in PBMCs but low in aortic

tissues), necessitating further experimental validation.

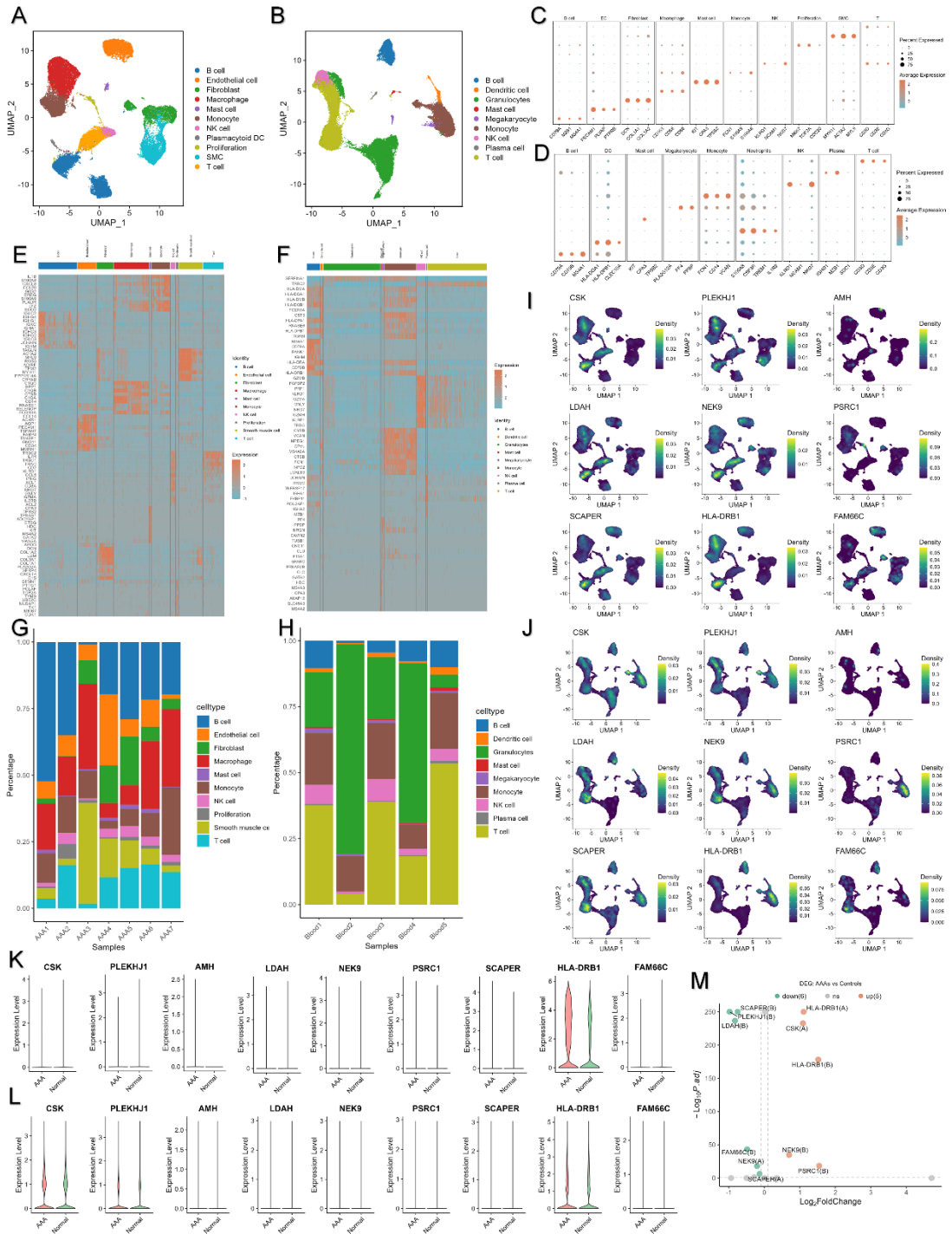


Figure 3. Cell Type Characterization and Expression Analysis of Causal Genes in AAA Tissue and PBMCs. UMAP plots of AAA tissue and PBMCs from AAA patients, respectively. (C-D) Dot plots displaying markers used to

annotate cell types in AAA aortic tissue and PBMCs. (E-F) Heatmaps showing the expression profiles of the top genes in different cell types within aortic tissue and PBMCs, respectively. (G) Bar plot of cell proportions across 7 AAA tissue samples. (H) Bar plot of cell proportions across 5 AAA PBMC samples. (I-J) Density plots of the expression distribution of 9 causal genes across different cell types in AAA tissue and PBMCs, respectively. (K) Expression levels of the 9 genes in AAA versus normal aortic tissue samples. (L) Expression levels of the 9 genes in AAA versus normal PBMC samples. (M) Differential expression analysis of the 9 genes in both tissue and PBMC samples overall. Teal color indicates lower expression relative to the control group, while orange-red indicates higher expression relative to the control group. Scatter points with the suffix 'A' represent differential expression in tissue, while those with the suffix 'B' represent differential expression in PBMCs.

3.3 Multi-Omics Landscape of Causal Genes in AAA

To summarize the multi-omics landscape of abdominal aortic aneurysm (AAA), we examined the GWAS-eQTL colocalization of nine genes alongside ATAC-seq data (for data processing details, **Figure S5A-I**). We selected a 200 kb window upstream and downstream of these genes (with adjustments made for longer gene sequences) to summarize high-confidence SNPs associated with AAA GWAS and their corresponding eQTLs, as well as ATAC-seq signal values and differential peaks. The results are visualized in **Figures 4A-C** and **Figure S6A-F**. Among the 9 genes, five demonstrated significant

colocalization with AAA GWAS in both aortic and PBMC eQTL datasets, including HLA-DRB1, LDAH, SCAPER, PLEKHJ1, and FAM66C. NEK9 showed significant colocalization only in the aortic eQTL, while the remaining three genes (CSK, AMH, and PSRC1) exhibited colocalization solely in the PBMC eQTL data. Notably, HLA-DRB1 and its neighboring genes exhibited higher ATAC-seq signal values in AAA samples compared to the control group (**Figure 4A**). Differential peaks were detected in the regions of LDAH and SCAPER, particularly a prominent differential peak located approximately 20.8 Mbp within the intronic region of LDAH, which was consistently identified across two replicates. The complete results of the differential peaks analysis are provided in **Supplementary File – Excel 6**, with no significant differential peaks found in the regions of the other six genes.

Next, we analyzed the expression profiles of the nine causal genes across different cell types in AAA. **Figures 4D-F** illustrate the expression levels of HLA-DRB1, LDAH, and SCAPER in aortic tissues, with feature plots on the left showing expression levels in AAA samples and those on the right showing expression in the control group. **Figures 4H-J** display their expression profiles in PBMCs. UMAP plots in **Figures 4G** and **Figure 4K** are provided for reference to the cell types in the feature plots. We employed the Wilcoxon test to assess whether there were significant differences in gene expression levels within each cell type. The expression profiles of the remaining six causal genes are presented in **Figure S7A-H**. The differential expression analyses for all genes in aortic tissues and PBMCs are shown in **Figure 4L** and **Figure 4M**, respectively. Genes with $|\log FC| > 0.5$ and $P < 0.05$ (Wilcoxon test) are plotted

as scatter points, with differentially expressed causal genes labeled accordingly (**Supplementary File – Excel 7**). HLA-DRB1 exhibited the most pronounced expression differences, showing high expression across various cell types in both aortic tissues and PBMCs, with the exception of low expression in B cells within the aortic tissues. HLA-DRB1 demonstrated significantly higher expression levels in cell types with strong associations to AAA, including macrophages, dendritic cells (DCs), fibroblasts, monocytes, and megakaryocytes, providing robust evidence for the causal link between high HLA-DRB1 expression and AAA. Furthermore, Mendelian randomization (MR) results indicated that low expression of SCAPER contributes to the development of AAA, as SCAPER was found to be downregulated in DCs, B cells, plasma cells, and T cells in AAA samples, further validating the causal relationship identified through MR. Similarly, PLEKHJ1 was found to be lowly expressed in various immune cells, and LDAH also exhibited low expression in DCs, which are strongly associated with AAA, thereby supporting their causal effects.

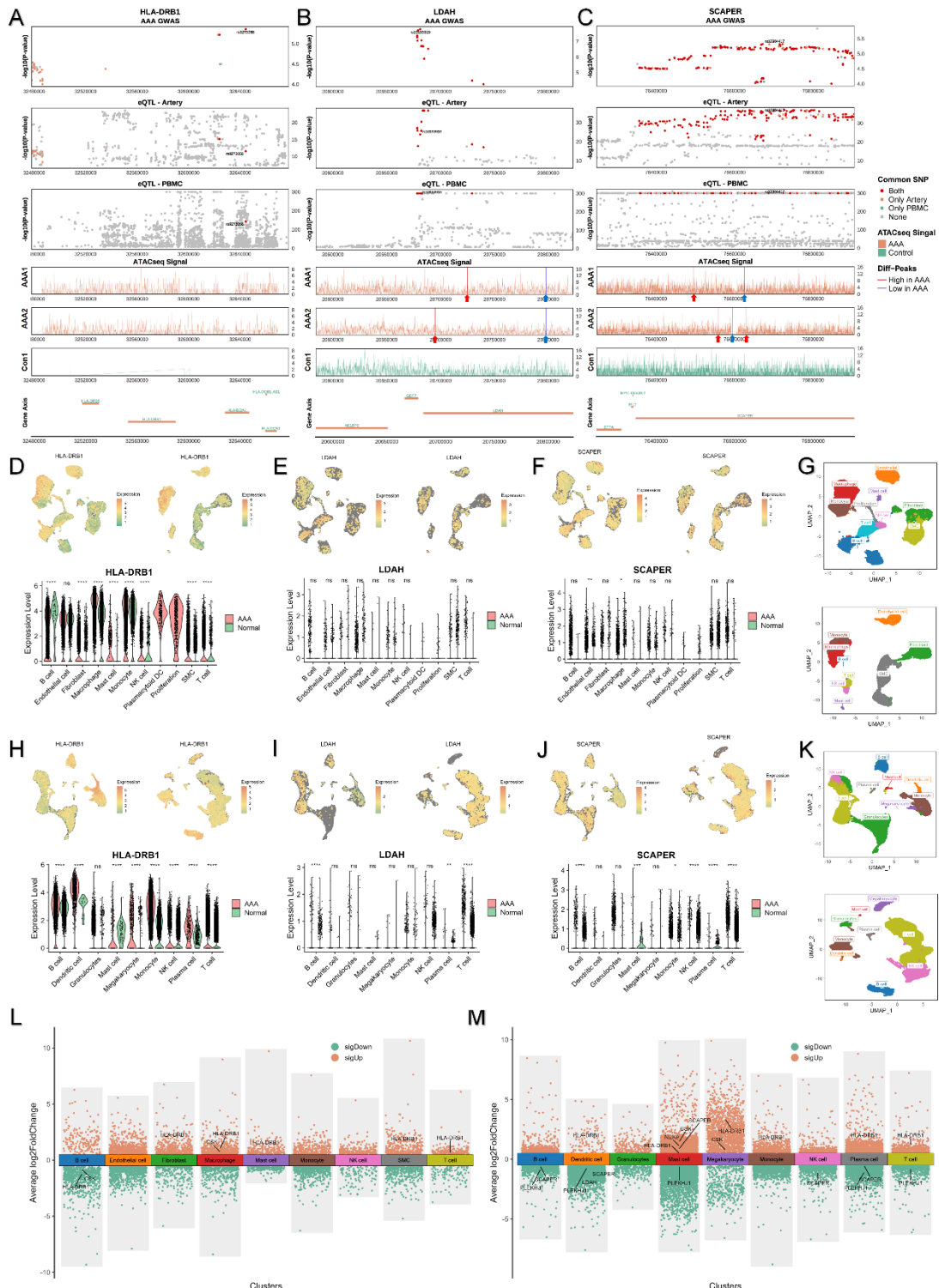


Figure 4. Colocalization and Expression Analysis of HLA-DRB1, LDAH, and SCAPER in AAA Tissue and PBMCs. Composite plots for HLA-DRB1, LDAH, and SCAPER gene regions depicting SNP colocalization and ATAC-seq signal levels. The first three panels within each composite plot

display SNP colocalization across AAA GWAS, aortic tissue eQTL (from GTEx), and PBMC eQTL. Each significant SNP within the region (GWAS threshold $P<1\times10^{-4}$, eQTL threshold $P<1\times10^{-8}$) is represented by a scatter point: red points indicate SNPs significantly colocalized in GWAS, aortic tissue eQTL, and PBMC eQTL simultaneously; orange-red points represent SNPs colocalized only in aortic tissue; blue points indicate SNPs colocalized only in PBMC; and gray points represent SNPs that are not colocalized. The three-line graphs depict ATAC-seq signal values, with regions marked by blue arrows and vertical lines indicating downregulated differential peaks in AAA, and red marks indicating upregulated peaks. The gene tracks for the region are shown at the bottom of each composite plot. (D-F) Expression profiles of HLA-DRB1, LDAH, and SCAPER in aortic tissue. The feature plots on the left are from AAA tissue, while those on the right are from normal aortic tissue. The violin plots below show the expression levels and differences (Wilcoxon test) of these genes across different cell types. (G) UMAP plots of cells within AAA and normal aortic tissue, used to compare cell types. (H-J) Expression profiles of the three genes in PBMCs. (K) UMAP plot of PBMCs. (L, M) Differential expression analysis in AAA tissue and PBMCs, showing genes with $|Log2(Fold Change)| > 0.5$ in each cell type. * $P<0.05$, ** $P<0.01$, *** $P<0.001$, **** $P<0.0001$

3.4 Enhanced MHC-II Signaling Pathway in Myeloid Immune Cells Drives AAA Development

The immune infiltration and inflammatory processes associated with the

MHC-II pathway are considered key factors in the development of abdominal aortic aneurysm (AAA). In our study, HLA-DRB1 was identified as having a unidirectional causal association with AAA, indicating that upregulation of HLA-DRB1 promotes AAA progression. Notably, HLA-DRB1 was found to be significantly overexpressed in myeloid cells within AAA tissues. Furthermore, cell-disease association analyses revealed stronger associations between myeloid cells in both tissue and PBMCs and AAA. Based on this evidence, we hypothesize that there is an aberration in the MHC-II signaling pathway in myeloid cells, which enhances immune infiltration and inflammatory responses in the aorta. To further investigate this, we utilized CellChat to analyze differences in MHC-II pathway communication levels between AAA patients and controls in both aortic tissues and PBMCs, corroborating our findings with proteomic data.

The CellChat analysis indicated a significant enhancement in overall communication levels among myeloid cells in AAA. In aortic tissues, both the quantity and intensity of communications were markedly higher in AAA compared to the control group (**Figure S8A**). With the exception of B cell communication and some communication from smooth muscle cells, the communication levels and strengths among other cell types were increased, particularly for signals emitted by fibroblasts, endothelial cells, and macrophages, as well as signals received by macrophages and NK cells (**Figures S8B** and **Figure S8C**). In PBMCs, while the overall quantity of cell communications was lower in AAA compared to controls, the communication intensity was higher (**Figure S8D**). Within the various cell types present in

PBMCs, signals related to myeloid cells, particularly those received by granulocytes and megakaryocytes, as well as signals emitted from myeloid cells to other myeloid cells, were significantly enhanced (**Figure S8E** and **Figure S8F**). The active communication among myeloid cells, fibroblasts, and endothelial cells in AAA aligns with the results from the cell-disease association analysis, highlighting their critical roles in the initiation and progression of AAA.

Next, we focused on the abnormal states of the MHC-II signaling pathway in AAA. **Figure 5A** and **Figure 5G** illustrate the relative information flow of signaling pathways in aortic tissues and PBMCs, respectively. Orange-red pathways indicate significantly higher information flow in AAA compared to the normal group, while blue-green indicates the opposite. Notably, the communication levels of the MHC-II signaling pathway were stronger in both aortic tissues and PBMCs of AAA patients compared to controls. The intercellular communication intensity and proportions of MHC-II in aortic tissues are depicted in **Figure 5B** and **Figure 5C**, respectively. We observed an upregulation of communication levels between T cells and macrophages, as well as between T cells and monocytes, in AAA, with a significant increase in signals emitted from monocyte-derived macrophages to T cells. Furthermore, the MHC-II signaling pathway in AAA was notably more active, involving a greater diversity of participating cell types. The expression levels of genes involved in the MHC-II signaling pathway are presented in **Figure 5D**, showing downregulation in B cells and upregulation in endothelial cells, macrophages, and monocytes in AAA. Importantly, HLA-DRB1 and HLA-DRA

were highly expressed in all cell types except B cells in AAA. The expression of the CD4 gene, a receptor for signaling, was predominantly found in macrophages, monocytes, and T cells, with expression levels in AAA being higher than in the normal group. The communication intensity between various HLA-II molecules and CD4 was enhanced in most cell types of AAA patients, particularly for signals emitted from B cells, endothelial cells, macrophages, and monocytes to macrophages, with signal strength measured by communication probability (**Figure 5E**). The signaling transduction involving HLA-DRB1, HLA-DRA, HLA-DPB1, and HLA-DPA1 was elevated across many different cell types in AAA, exhibiting stronger communication relative to other signaling pathways. Conversely, there were fewer downregulated signals in the MHC-II signaling pathway in AAA, with notable exceptions being multiple signals from B cells to monocytes (**Figure 5F**).

In PBMCs, the overall intensity of the MHC-II signaling pathway was higher in AAA patients, with a greater variety of participating cell types, particularly showing significant enhancement in communication levels among monocytes, megakaryocytes, and dendritic cells compared to controls (**Figure 5H** and **Figure 5I**). Similar to aortic tissues, HLA-DRB1, HLA-DRA, HLA-DPB1, and HLA-DPA1 exhibited high expression in various cell types within the PBMCs of AAA patients, while the receptor CD4 was also significantly more expressed in monocytes, megakaryocytes, and dendritic cells compared to controls. In contrast, CD4 expression in T cells was lower in AAA patients than in the normal group, likely due to chronic inflammation and local immune infiltration leading to overall T cell functional exhaustion, consistent with the notably

reduced number and proportion of T cells in the PBMCs of AAA patients (**Figure 5J**). The widespread high expression of these four HLA-II molecules contributes to the broad upregulation of their associated signaling pathways. Additionally, signaling pathways involving monocytes, megakaryocytes, and dendritic cells were also widely upregulated and intersected with the signals mediated by the four highly expressed HLA-II molecules (**Figure 5K**). Furthermore, similar to aortic tissues, there were fewer downregulated signals in the MHC-II pathway in AAA, primarily involving dendritic cells and monocytes receiving signals from other immune cell types (**Figure 5L**).

HLA-DRA and HLA-DRB1 encode the alpha and beta chains of MHC II molecules, respectively, with these two chains forming a heterodimer that binds and presents antigens, thus playing a core role in immune responses. Single-cell sequencing results showed significant overexpression of these molecules not only in the aortic tissues of AAA patients but also in various cell types within PBMCs. To further elucidate the changes in the abundance of MHC II molecules within AAA tissues, we conducted a proteomic analysis, including two AAA group samples (for AAA n=10, for rAAA n=10) and a normal group (n=10) sample (**Supplementary File – Table 2**). Differential analysis between the two AAA samples and the control group was performed, identifying proteins with fold change > 1.2 and $P < 0.05$ as significantly different. The results are detailed in **Supplementary File – Excel 8**. In AAA group, we identified 206 downregulated proteins and 213 upregulated proteins, while rAAA group showed 191 downregulated proteins and 204 upregulated proteins (**Figure 5M**). A total of 176 proteins were consistently upregulated

across both samples, while 179 proteins were consistently downregulated (**Figure 5N**). The scatter plot in **Figure 5O** illustrates the fold changes of all differential proteins across the two replicates, with HLA class II DR α proteins showing upregulation (fold changes of 1.313 and 1.247, respectively). Differential proteins interacting with HLA class II DR α are shown in **Figure 5P**, with orange-red indicating upregulation and blue-green indicating downregulation. Notably, complement components C1qA, C1qB, and C1qC were all upregulated in AAA, forming a petal-like structure of the C1 complex, and protein interaction analyses from the STRING database indicated interactions between these components and HLA class II DR α . Furthermore, the C1 complex can bind to antibody-antigen complexes, activating the classical complement pathway, thereby promoting the uptake and antigen presentation of HLA-II molecules by macrophages and dendritic cells.

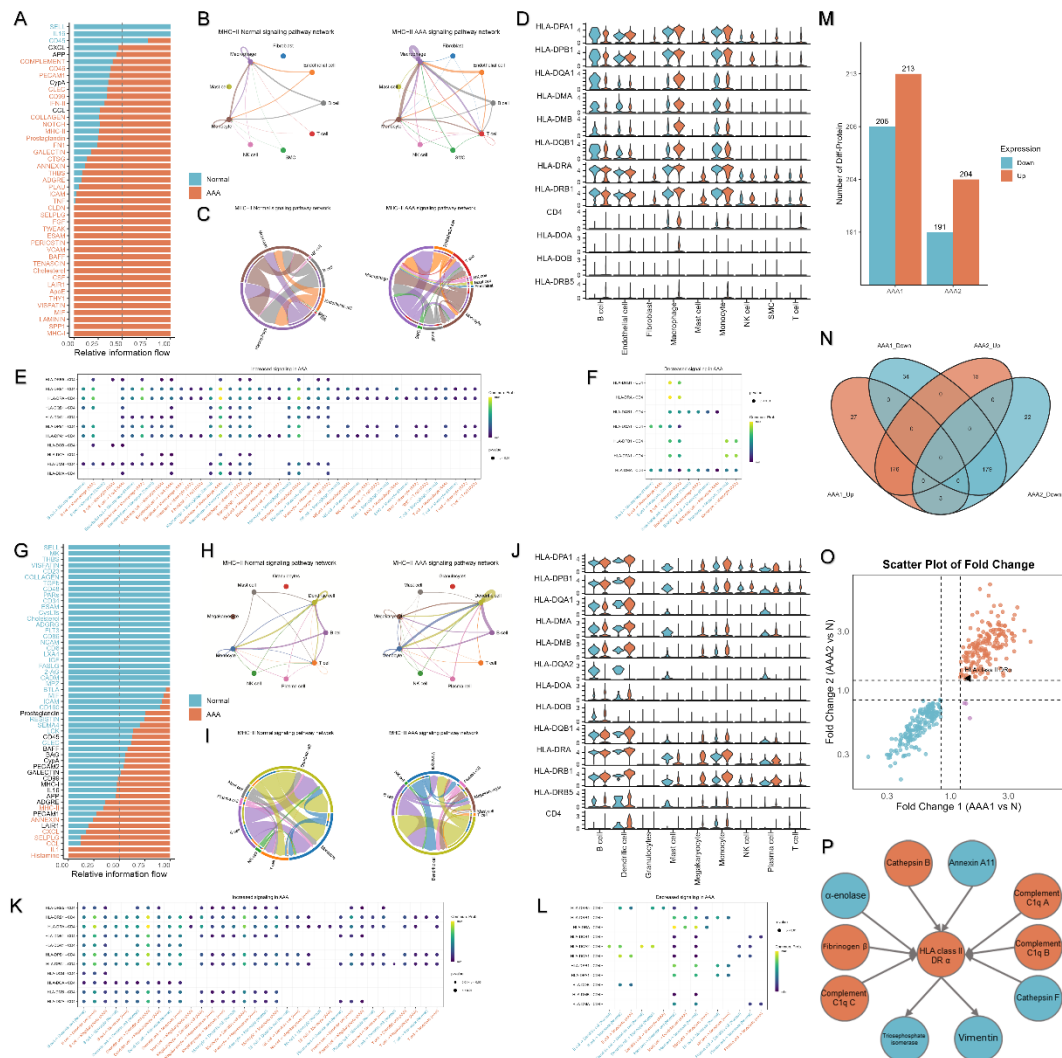


Figure 5. Differential Pathways of Cell-Cell Communication and MHC-II

Signaling in AAA Aortic Tissue and PBMCs. (A) Differential pathways of cell-cell communication in aortic tissue. The x-axis represents the relative information flow between the AAA and normal groups, with orange-red indicating upregulation in AAA and teal indicating downregulation in AAA. (B) Network diagram of MHC-II signaling pathways between cells, where the width of the connections represents the strength of communication. (C) Chord diagram showing the relative strength of MHC-II signaling pathways between cells. (D) Violin plots displaying the expression levels and differences of MHC-II signaling-related genes across different cell types in aortic tissue, blue

represents normal samples, while red indicates samples associated with AAA. (E, F) Upregulated and downregulated signals in AAA aortic tissue, respectively. The closer the color of the dots is yellow, the higher the probability value and communication level. (G-L) Intercellular communication of the MHC-II pathway in AAA PBMCs and the differences compared to the control group, similar to the content shown in the aortic tissue plots. (M) Bar chart showing the number of differentially expressed proteins in the proteomics analysis. (N) Venn diagram illustrating the intersection of differentially expressed proteins in two replicates. (O) Scatter plot showing genes that were differentially expressed in both replicates, with the x and y axes representing fold change (FC > 1.2 considered significant). Orange-red dots represent proteins that were upregulated in both replicates, while teal dots represent proteins that were downregulated in both. (P) Interaction network of differentially expressed proteins interacting with HLA class II DR α protein, with orange-red indicating proteins upregulated in both replicates and teal indicating proteins downregulated in both.

3.5 Causal Genes in CMU aneurysm Biobank via Experimental Verification

Further, we validated these gene hypotheses through biological experiments. In human tissue samples, we utilized immunofluorescence (IF) and found that, compared to normal individuals, HLA-DRB1 was highly expressed in patients with abdominal aortic aneurysm (AAA), with this expression predominantly localized in the tunica media and tunica adventitia (**Figure 6A, and 6B**). Subsequently, we co-localized it with the macrophage surface marker CD68

and observed a strong overlap with macrophage markers. At the protein expression level, Western blot analysis revealed a significantly elevated expression of HLA-DRB1 in AAAs ($P = 0.0013$, **Figure 6C**). Similarly, AMH also showed a high expression trend in the tunica adventitia and tunica media of AAA (**Figure 6D**), a phenomenon not observed in normal individuals (**Figure 6E**). Western blot analysis confirmed this significant upregulation ($P = 0.0085$, **Figure 6F**). For protein expression, such as CSK, NEK9, and LDAH, which previously exhibited a negative correlation, immunohistochemistry and Western blotting demonstrated that CSK showed a trend of low expression in the immunohistochemical analysis (**Figure 6G**), and this was further corroborated by Western blotting ($P = 0.0001$, **Figure 6H**). NEK9, which encodes NimA, also exhibited consistent and significantly low expression ($P = 0.0013$, **Figure 6I**, and **6J**). The gene related to lipid droplet-associated hydrolase activity (LDAH) also displayed a significant decrease in expression ($P = 0.0047$, **Figure 6K**, and **6L**). These findings are consistent with our previous predictions, confirming a critical relationship with the development and progression of AAA. In terms of tissue morphology, The Hematoxylin and Eosin (H&E) staining revealed a thickened vascular wall in AAAs, with disruptions observed in the intima and media (**Figure 6M**). The adventitia exhibited inflammatory infiltration, along with an increased presence of neovascularization. The results of the Elastic van Gieson (EvG) staining indicated that the elastic fibers were disrupted due to pathological changes, leading to a widening of the gaps between the fibers (**Figure 6N**). Compared to the control group, there was a greater amount of collagen fibers and inflammatory cell infiltration. Moreover, at the mRNA level, we performed

real-time quantitative PCR on tissues from AAA patients and normal individuals. The results showed that the relative expression levels of HLA-DRB1 and AMH were upregulated in the AAA group, whereas SCAPER, LDAH, NEK9, PSRC1, and PLEKJH1 exhibited a relatively downregulated trend (Figure 6O).

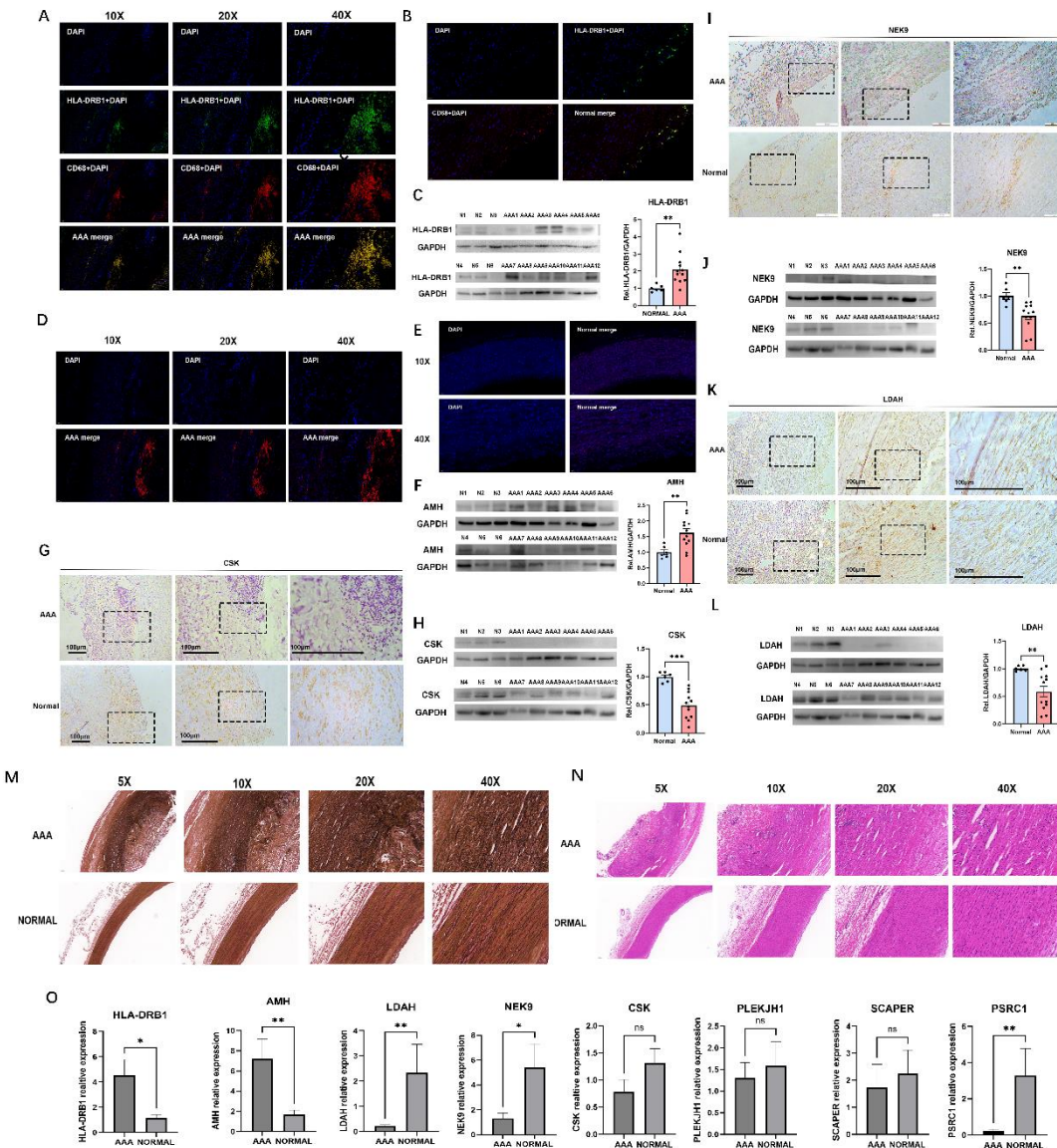


Figure 6. Immunofluorescence and Expression Analysis of HLA-DRB1, AMH, CSK, NEK9, and LDAH in Human AAA Tissue. IF staining results of

human AAA samples at different magnifications (10X, 20X, 40X). The blue regions represent cell nuclei stained with DAPI, while green and red indicate the specific expression of HLA-DRB1 and the macrophage marker CD68, respectively. The overlapping areas suggest interactions between macrophages and HLA-DRB1 in human AAAs (A); Co-localization of CD68 and HLA-DRB1 in normal human samples (B); Western blot analysis showing the expression of HLA-DRB1 in AAA and normal tissues (C); IF staining results of human AAA samples at different magnifications (10X, 20X, 40X), with red fluorescence representing the target gene AMH (D). DAPI (blue) and target gene²¹ staining of normal human samples at 10X and 40X magnification (E); Western blot analysis showing the expression of AMH in AAA and normal tissues (F); Immunohistochemistry (IHC) staining of CSK, scale bar = 100 µm (G); CSK protein expression in AAA and normal tissues (H); IHC staining of NEK9, scale bar = 100 µm (I); NEK9 protein expression in AAA and normal tissues (J); IHC staining of LDAH, scale bar = 100 µm(K); LDAH expression in AAA and normal tissues (L); Histological staining results of EVG between AAA and NORMAL (M); HE staining results between abdominal aortic aneurysm and normal tissue(N) qPCR results of aortic tissues from AAA patients and normal individuals, measured using the $2^{-(\Delta\Delta CT)}$ method to determine relative expression levels (O). Data are presented as mean ± SEM, (Normal n = 6 and AAA n = 12). DAPI represents 4',6-diamidino-2-phenylindole. Representative images of immunofluorescence staining. *P < 0.05, **P < 0.01, ***P < 0.001, ****P < 0.0001

4. Discussion

The GWAS identified several novel genetic loci associated with abdominal aortic aneurysm (AAA), many of which are located near genes involved in vascular development and remodeling, extracellular matrix organization, and inflammation^{22,23}. These loci provide new insights into the genetic architecture of AAA and highlight potential biological pathways involved in its pathogenesis²⁴. The scRNA-seq data revealed significant cellular heterogeneity within AAA tissues, with distinct cell populations exhibiting unique gene expression profiles²⁵. This heterogeneity underscores the complexity of AAA and the need for targeted therapeutic approaches that consider the diverse cellular landscape of the disease. The ATAC-seq analysis identified key regulatory elements that are differentially accessible in AAA tissues. These regulatory elements are likely to play crucial roles in modulating gene expression in response to pathological stimuli, providing potential targets for therapeutic intervention. This study identified nine genes with causal effects on AAA through comprehensive genetic analysis, including GWAS, Mendelian randomization, and Bayesian colocalization. Among these, HLA-DRB1 and AMH were found to increase the risk of AAA, while LDAH, NEK9, and others were protective. Single-cell transcriptomics revealed that HLA-DRB1 is significantly overexpressed in immune cells within AAA tissues, particularly in myeloid cells, highlighting its role in immune-mediated pathogenesis. Additionally, the study demonstrated that the MHC-II signaling pathway, particularly involving HLA-DRB1, is markedly enhanced in AAA, promoting immune infiltration and inflammation. These findings suggest that targeting specific genes and immune pathways could offer new therapeutic strategies

for managing AAA.

We also investigated the role of NIMA-related kinase 9 (NEK9) in AAA. Existing studies have identified NEK9 as a crucial regulator of human essential myosin light chain (ELC) phosphorylation in a calcium-dependent manner, highlighting its importance in cardiac function and disease. Specifically, NEK9 interacts with ELC through its protein kinase domain, and its silencing results in reduced calcium-dependent ELC phosphorylation. Furthermore, disruption of NEK9 in zebrafish leads to cardiomyopathy, demonstrating its critical role in maintaining cardiac health²⁶. Increased ELC phosphorylation in patients with dilated cardiomyopathy further underscores NEK9's involvement in cardiovascular diseases. Our study extends these insights into the context of AAA. We found that NEK9 acts as a protective factor in AAA, with both mRNA and protein levels of NEK9 significantly lower in AAA tissues compared to normal abdominal aorta tissues. This reduction in NEK9 expression in AAA suggests that NEK9's protective mechanisms may be compromised in this disease. The protective role of NEK9 in AAA may be linked to its regulatory functions in cardiac contraction and inotropy. By mediating calcium-dependent phosphorylation of ELC, NEK9 helps maintain proper vascular function, which is critical for adapting to changing hemodynamic demands. The diminished expression of NEK9 in AAA could potentially impair these regulatory mechanisms, contributing to the pathophysiology of AAA.

Furthermore, we explored the role of Anti-Müllerian hormone (AMH) in AAA. Previous studies have identified AMH as a potential regulator of cardiovascular

health, with high AMH levels associated with a lower incidence of cardiovascular disease in men and reduced atherosclerotic burden in animal models²⁷. They also found that serum AMH levels inversely correlated with the diameter of the distal and mid-infrarenal aorta, independent of other cardiovascular risk factors. However, there is limited research specifically examining the relationship between AMH and AAA, with only one study to date suggesting AMH as a protective factor. Contrary to this previous report, our GWAS combined with Mendelian randomization analysis revealed that AMH acts as a risk factor for AAA. Our experimental validation demonstrated that both mRNA and protein levels of AMH were significantly higher in AAA tissues compared to normal abdominal aorta tissues. This elevated expression of AMH in AAA suggests a pathogenic role, contrasting with its purported protective functions in other cardiovascular contexts. Our findings indicate that the relationship between AMH and cardiovascular health is complex and context-dependent. While high levels of AMH have been associated with reduced aortic diameters in healthy men, our data suggest that in the context of AAA, elevated AMH levels may contribute to disease progression. The mechanisms underlying this dual role of AMH remain to be fully elucidated, but it is possible that AMH influences different pathways or cellular processes in the aorta under pathological conditions. Two additional studies support the complex role of AMH in cardiovascular health. One long-term cohort study with 3,108 women found that lower AMH levels were associated with an increased risk of cardiovascular disease (CVD) and coronary heart disease, suggesting a protective role of higher AMH levels²⁸. Another systematic review of 37 observational studies reported an inverse relationship between AMH and

adverse lipid profiles, with mixed results regarding glycemic parameters and adiposity indices, but some evidence of an association between AMH and vascular markers like intima-media thickness²⁹. The presence of AMH receptors in the aorta further supports the notion that AMH can directly affect vascular tissues. The specific pathways through which AMH exerts its effects in AAA need to be investigated, including its interactions with other cardiovascular regulators and its impact on vascular cell function and integrity.

Our study also has highlighted the pivotal role of the MHC-II signaling pathway and the HLA-DRB1 gene in the pathogenesis of AAA. The enhanced activity of the MHC-II pathway in myeloid cells and the upregulation of HLA-DRB1 across various immune cell types underscore the immune-mediated nature of AAA development and progression. HLA-DRB1 encodes the beta chain of the MHC-II complex in humans, with MHC-II molecules primarily expressed on the surface of specialized antigen-presenting cells, such as macrophages and dendritic cells³⁰. The MHC-II-mediated signaling pathway is a crucial signaling cascade within the immune system. CD4⁺ T cells recognize and bind to MHC-II-antigen complexes through their T cell receptors (TCRs), leading to the activation of CD4⁺ T cells and the downstream activation of pathways such as PI3K-Akt and MAPK³¹. Mexican study found that specific alleles of the Class II Human Leukocyte Antigens (HLA-DRB1), particularly HLA-DRB1*01 and HLA-DRB1*16, are linked to a higher risk of AAA in the Mexican Mestizo population. The allele frequency of HLA-DRB1*01 was 0.139 in AAA patients, significantly higher than 0.05 in the control group. Similarly, HLA-DRB1*16 had a frequency of 0.109 in AAA patients versus 0.025 in controls ($P = 0.006$).

These findings suggest that genetic testing for these alleles could help identify individuals at increased risk for AAA, enabling earlier screening and closer monitoring³². However, a UK study investigated the distribution of HLA alleles in AAA patients compared to controls and found no significant differences after Bonferroni correction. HLA-DRB1*11 and *14 was less common in large AAAs, but this was not significant after correction. Thus, HLA-DRB1 alleles do not appear to play a crucial role in AAA etiology as previously suggested³³. In this study, we also found the communication intensity between various HLA-II molecules and CD4⁺ was enhanced in most cell types of AAA patients, particularly for signals emitted from B cells, endothelial cells, macrophages, and monocytes to macrophages. The MHC-II pathway is central to the immune system's ability to present antigens and activate CD4⁺ T cells, which in turn drive the immune response³⁴. In the context of AAA, our results demonstrated that the MHC-II signaling was significantly upregulated, particularly within myeloid cells, including macrophages and dendritic cells. This upregulation was not only observed in the aortic tissue but also in peripheral blood mononuclear cells (PBMCs) from AAA patients. The increased MHC-II pathway activity likely contributes to the heightened immune cell infiltration observed in the aneurysmal aorta. The data from single-cell RNA sequencing (scRNA-seq) provided compelling evidence that myeloid cells within the aneurysmal tissue were actively engaging in antigen presentation, which could be driving a local, chronic inflammatory response. This response is characterized by the recruitment and activation of T cells and other immune cells, leading to the progression of the aneurysm. HLA-DRB1, which encodes the β-chain of the MHC class II molecule, emerged as a gene of significant

interest due to its consistent upregulation in AAA-associated immune cells. Our Mendelian randomization (MR) analysis indicated that increased expression of HLA-DRB1 is causally related to a higher risk of AAA, suggesting that HLA-DRB1 could be a key driver of the pathogenic immune responses observed in AAA. The overexpression of HLA-DRB1 in myeloid cells, particularly in macrophages and dendritic cells, points to a scenario where these cells might be excessively presenting autoantigens or neoantigens generated in the context of vascular inflammation or damage. This could lead to a self-sustaining cycle of immune activation and tissue remodeling, further exacerbating the aneurysmal dilation. Moreover, the proteomic analysis revealed that HLA class II molecules, including HLA-DRA (encoded by HLA-DRA) and HLA-DR β (encoded by HLA-DRB1), were not only upregulated but also showed increased interactions with components of the complement system, such as C1q. This interaction suggests a possible link between the MHC-II pathway and the classical complement pathway in driving the inflammatory response within the aneurysmal wall. The aberrant activation of the MHC-II pathway in AAA could be driven by several mechanisms. One possibility is the presence of chronic infections or persistent vascular injury that leads to continuous antigen presentation and T cell activation³⁵. Alternatively, genetic factors, such as specific polymorphisms in the HLA-DRB1 gene, might predispose individuals to an exaggerated immune response, thereby increasing their risk of developing AAA. Understanding the exact triggers of MHC-II pathway activation in AAA is crucial for developing targeted therapies. Given the central role of HLA-DRB1, therapeutic strategies that modulate its expression or function could potentially mitigate the immune-driven

progression of AAA. For instance, targeting the antigen-presenting function of HLA-DRB1 in myeloid cells might reduce T cell activation and the subsequent inflammatory cascade, offering a novel approach to slow down or prevent AAA progression.

This study explored the impact of noncoding SNPs on endothelial cell function and vascular disease risk. Using the STARR-seq assay, 5711 variants were identified as functional, with notable features such as alterations in transcription factor binding motifs and chromatin accessibility. Specifically, noncoding SNPs at the LDAH locus were found to influence the risk of abdominal aortic aneurysm by affecting transcriptional regulation. These findings emphasize the importance of noncoding genetic variation in vascular disease mechanisms³⁶. Atherosclerosis and AAA are both major vascular diseases that often co-exist and share several underlying pathophysiological mechanisms. Goo et al. et al identified LD-associated hydrolase (LDAH) as a key regulator of cholesterol trafficking in macrophage foam cells. Proteomic analysis confirmed LDAH association with lipid droplets and its role in cholesterol ester (CE) homeostasis. Upregulation of LDAH enhances CE hydrolysis and cholesterol efflux from macrophages, suggesting LDAH as a potential target for promoting reverse cholesterol transport in atherosclerotic lesions³⁷. Atherosclerosis is characterized by the accumulation of lipids, inflammatory cells, and fibrous elements in the arterial walls, leading to the formation of plaques. Dyslipidemia is a common risk factor for both diseases. In atherosclerosis, low-density lipoprotein (LDL) cholesterol accumulates in the arterial wall, where it undergoes oxidation and triggers an inflammatory

response. In AAA, lipid accumulation within the aortic wall can also contribute to inflammation and ECM degradation³⁸. Genetic predispositions can influence the development of both atherosclerosis and AAA. For instance, variations in genes related to lipid metabolism, inflammation, and ECM structure can affect individual susceptibility to both conditions. Recent studies have identified noncoding SNPs, such as those affecting LDAH, that influence the risk of both vascular diseases through transcriptional regulation mechanisms. This reinforces the significance of noncoding SNPs at the LDAH locus, previously highlighted for their role in vascular disease risk, specifically abdominal aortic aneurysm.

5. Conclusion

This study provides a comprehensive multi-omic analysis of AAA, integrating genetic, transcriptomic, and epigenomic data to elucidate the molecular mechanisms driving the AAAs. Our findings establish the MHC-II pathway, particularly HLA-DRB1, as critical components in the immune-mediated pathogenesis of AAA. The strong association between HLA-DRB1 expression and AAA risk, coupled with the pathway's role in immune cell activation and inflammation, highlights its potential as a therapeutic target. In summary, this study highlights the power of integrative multi-omic approaches in unraveling the genetic and molecular basis of complex diseases like AAA, paving the way for precision medicine and targeted therapies. Further research into the modulation of this pathway could pave the way for new treatments aimed at preventing or treating AAA by curbing the immune-mediated damage that

underlies this condition.

6. References

1. Stather PW, Sidloff DA, Rhema IA, Choke E, Bown MJ, Sayers RD. A review of current reporting of abdominal aortic aneurysm mortality and prevalence in the literature. *Eur J Vasc Endovasc Surg.* 2014;47:240-242. doi: 10.1016/j.ejvs.2013.11.007
2. Kuivaniemi H, Elmore JR. Opportunities in abdominal aortic aneurysm research: epidemiology, genetics, and pathophysiology. *Ann Vasc Surg.* 2012;26:862-870. doi: 10.1016/j.avsg.2012.02.005
3. Vijaykumar K, Choke E. Shared Decision Making for Abdominal Aortic Aneurysm: Patients Want It But Are Not Getting It. *Eur J Vasc Endovasc Surg.* 2023;65:850. doi: 10.1016/j.ejvs.2023.02.008
4. Pinard A, Jones GT, Milewicz DM. Genetics of Thoracic and Abdominal Aortic Diseases. *Circ Res.* 2019;124:588-606. doi: 10.1161/CIRCRESAHA.118.312436
5. Steffen BT, Pankow JS, Norby FL, Lutsey PL, Demmer RT, Guan W, Pankratz N, Li A, Liu G, Matsushita K, et al. Proteomics Analysis of Genetic Liability of Abdominal Aortic Aneurysm Identifies Plasma Neogenin and Kit Ligand: The ARIC Study. *Arterioscler Thromb Vasc Biol.* 2023;43:367-378. doi: 10.1161/ATVBAHA.122.317984
6. Bradley DT, Badger SA, McFarland M, Hughes AE. Abdominal Aortic Aneurysm Genetic Associations: Mostly False? A Systematic Review and Meta-analysis. *Eur J Vasc Endovasc Surg.* 2016;51:64-75. doi:

10.1016/j.ejvs.2015.09.006

7. Jones GT, Tromp G, Kuivaniemi H, Gretarsdottir S, Baas AF, Giusti B, Strauss E, Van't Hof FN, Webb TR, Erdman R, et al. Meta-Analysis of Genome-Wide Association Studies for Abdominal Aortic Aneurysm Identifies Four New Disease-Specific Risk Loci. *Circ Res*. 2017;120:341-353. doi: 10.1161/CIRCRESAHA.116.308765
8. Aneurysm C. Genome Wide Association Studies: identifying the genes that determine the risk of abdominal aortic aneurysm. *Eur J Vasc Endovasc Surg*. 2008;36:395-396. doi: 10.1016/j.ejvs.2008.06.003
9. Maimaiti A, Turhon M, Abulaiti A, Dilixiati Y, Zhang F, Axieer A, Kadeer K, Zhang Y, Maimaitili A, Yang X. DNA methylation regulator-mediated modification patterns and risk of intracranial aneurysm: a multi-omics and epigenome-wide association study integrating machine learning, Mendelian randomization, eQTL and mQTL data. *J Transl Med*. 2023;21:660. doi: 10.1186/s12967-023-04512-w
10. Lv Y, Shen D, Zhang G, Wang B, Wang H, Zhang J, Tang J. Causal Associations Between the Gut Microbiome and Aortic Aneurysm: A Mendelian Randomization Study. *CVIA*. 2024;9. doi: 10.15212/cvia.2024.0023
11. Chen Y, Xu X, Wang L, Li K, Sun Y, Xiao L, Dai J, Huang M, Wang Y, Wang DW. Genetic insights into therapeutic targets for aortic aneurysms: A Mendelian randomization study. *EBioMedicine*. 2022;83:104199. doi: 10.1016/j.ebiom.2022.104199
12. Le S, Wu J, Liu H, Du Y, Wang D, Luo J, Yang P, Ran S, Hu P, Chen M, et al. Single-cell RNA sequencing identifies IFNICs as a cellular target

- for mitigating the progression of abdominal aortic aneurysm and rupture risk. *Cardiovasc Res.* 2024. doi: 10.1093/cvr/cvae117
13. Zhao G, Lu H, Chang Z, Zhao Y, Zhu T, Chang L, Guo Y, Garcia-Barrio MT, Chen YE, Zhang J. Single-cell RNA sequencing reveals the cellular heterogeneity of aneurysmal infrarenal abdominal aorta. *Cardiovasc Res.* 2021;117:1402-1416. doi: 10.1093/cvr/cvaa214
 14. Yu L, Zhang J, Gao A, Zhang M, Wang Z, Yu F, Guo X, Su G, Zhang Y, Zhang M, et al. An intersegmental single-cell profile reveals aortic heterogeneity and identifies a novel Malat1(+) vascular smooth muscle subtype involved in abdominal aortic aneurysm formation. *Signal Transduct Target Ther.* 2022;7:125. doi: 10.1038/s41392-022-00943-x
 15. Tong Z, Mang G, Wang D, Cui J, Yang Q, Zhang M. Single-Cell RNA Sequencing Maps Immune Cell Heterogeneity in Mice with Allogeneic Cardiac Transplantation. *CVIA.* 2023;8. doi: 10.15212/cvia.2023.0023
 16. Ranzoni AM, Tangherloni A, Berest I, Riva SG, Myers B, Strzelecka PM, Xu J, Panada E, Mohorianu I, Zaugg JB, et al. Integrative Single-Cell RNA-Seq and ATAC-Seq Analysis of Human Developmental Hematopoiesis. *Cell Stem Cell.* 2021;28:472-487 e477. doi: 10.1016/j.stem.2020.11.015
 17. Zhang L, Yang H, Zhou C, Li Y, Long Z, Li Q, Zhang J, Qin X. Artificial intelligence-driven multiomics predictive model for abdominal aortic aneurysm subtypes to identify heterogeneous immune cell infiltration and predict disease progression. *Int Immunopharmacol.* 2024;138:112608. doi: 10.1016/j.intimp.2024.112608
 18. Giambartolomei C, Vukcevic D, Schadt EE, Franke L, Hingorani AD,

- Wallace C, Plagnol V. Bayesian test for colocalisation between pairs of genetic association studies using summary statistics. *PLoS Genet.* 2014;10:e1004383. doi: 10.1371/journal.pgen.1004383
19. Tang D, Han Y, Lun Y, Jiang H, Xin S, Duan Z, Zhang J. Y chromosome loss is associated with age-related male patients with abdominal aortic aneurysms. *Clin Interv Aging.* 2019;14:1227-1241. doi: 10.2147/CIA.S202188
20. He Y, Xing J, Wang S, Xin S, Han Y, Zhang J. Increased m6A methylation level is associated with the progression of human abdominal aortic aneurysm. *Ann Transl Med.* 2019;7:797. doi: 10.21037/atm.2019.12.65
21. The GC, Aguet F, Anand S, Ardlie KG, Gabriel S, Getz GA, Graubert A, Hadley K, Handsaker RE, Huang KH, et al. The GTEx Consortium atlas of genetic regulatory effects across human tissues. *Science.* 2020;369:1318-1330. doi: 10.1126/science.aaz1776
22. Zheng S, Tsao PS, Pan C. Abdominal aortic aneurysm and cardiometabolic traits share strong genetic susceptibility to lipid metabolism and inflammation. *Nat Commun.* 2024;15:5652. doi: 10.1038/s41467-024-49921-7
23. Qin T, Zhong J, Li P, Liang J, Li M, Zhang G. Matrix Metalloproteinase and Aortic Aneurysm: A Two-sample Mendelian Randomization Study. *Ann Vasc Surg.* 2024;105:227-235. doi: 10.1016/j.avsg.2024.02.011
24. Roychowdhury T, Klarin D, Levin MG, Spin JM, Rhee YH, Deng A, Headley CA, Tsao NL, Gellatly C, Zuber V, et al. Genome-wide association meta-analysis identifies risk loci for abdominal aortic

- aneurysm and highlights PCSK9 as a therapeutic target. *Nat Genet.* 2023;55:1831-1842. doi: 10.1038/s41588-023-01510-y
25. Davis FM, Tsoi LC, Ma F, Wasikowski R, Moore BB, Kunkel SL, Gudjonsson JE, Gallagher KA. Single-cell Transcriptomics Reveals Dynamic Role of Smooth Muscle Cells and Enrichment of Immune Cell Subsets in Human Abdominal Aortic Aneurysms. *Ann Surg.* 2022;276:511-521. doi: 10.1097/SLA.0000000000005551
26. Muller M, Eghbalian R, Boeckel JN, Frese KS, Haas J, Kayvanpour E, Sedaghat-Hamedani F, Lackner MK, Tugrul OF, Ruppert T, et al. NIMA-related kinase 9 regulates the phosphorylation of the essential myosin light chain in the heart. *Nat Commun.* 2022;13:6209. doi: 10.1038/s41467-022-33658-2
27. Dennis NA, Jones GT, Chong YH, van Rij AM, McLennan IS. Serum anti-Mullerian hormone (AMH) levels correlate with infrarenal aortic diameter in healthy older men: is AMH a cardiovascular hormone? *J Endocrinol.* 2013;219:13-20. doi: 10.1530/JOE-13-0125
28. de Kat AC, Verschuren WM, Eijkemans MJ, Broekmans FJ, van der Schouw YT. Anti-Mullerian Hormone Trajectories Are Associated With Cardiovascular Disease in Women: Results From the Doetinchem Cohort Study. *Circulation.* 2017;135:556-565. doi: 10.1161/CIRCULATIONAHA.116.025968
29. Fallahzadeh A, Ramezeni Tehrani F, Rezaee M, Mahboobifard F, Amiri M. Anti-Mullerian hormone and cardiometabolic status: a systematic review. *Biomarkers.* 2023;28:486-501. doi: 10.1080/1354750X.2023.2223365

30. van Drongelen V, Scavuzzi BM, Nogueira SV, Miller FW, Sawalha AH, Holoshitz J. HLA-DRB1 allelic epitopes that associate with autoimmune disease risk or protection activate reciprocal macrophage polarization. *Sci Rep.* 2021;11:2599. doi: 10.1038/s41598-021-82195-3
31. De Riva A, Bourgeois C, Kassiotis G, Stockinger B. Noncognate interaction with MHC class II molecules is essential for maintenance of T cell metabolism to establish optimal memory CD4 T cell function. *J Immunol.* 2007;178:5488-5495. doi: 10.4049/jimmunol.178.9.5488
32. Anaya-Ayala JE, Hernandez-Dono S, Escamilla-Tilch M, Marquez-Garcia J, Hernandez-Sotelo K, Lozano-Corona R, Ruiz-Gomez D, Granados J, Hinojosa CA. Genetic polymorphism of HLA-DRB1 alleles in Mexican mestizo patients with abdominal aortic aneurysms. *BMC Med Genet.* 2019;20:102. doi: 10.1186/s12881-019-0833-8
33. Badger SA, Soong CV, O'Donnell ME, Middleton D. The role of human leukocyte antigen genes in the formation of abdominal aortic aneurysms. *J Vasc Surg.* 2007;45:475-480. doi: 10.1016/j.jvs.2006.09.067
34. Couture A, Garnier A, Docagne F, Boyer O, Vivien D, Le-Mauff B, Latouche JB, Toutirais O. HLA-Class II Artificial Antigen Presenting Cells in CD4(+) T Cell-Based Immunotherapy. *Front Immunol.* 2019;10:1081. doi: 10.3389/fimmu.2019.01081
35. Lintermans LL, Stegeman CA, Heeringa P, Abdulahad WH. T cells in vascular inflammatory diseases. *Front Immunol.* 2014;5:504. doi: 10.3389/fimmu.2014.00504
36. Toropainen A, Stolze LK, Ord T, Whalen MB, Torrell PM, Link VM,

- Kaikkonen MU, Romanoski CE. Functional noncoding SNPs in human endothelial cells fine-map vascular trait associations. *Genome Res.* 2022;32:409-424. doi: 10.1101/gr.276064.121
37. Goo YH, Son SH, Kreienberg PB, Paul A. Novel lipid droplet-associated serine hydrolase regulates macrophage cholesterol mobilization. *Arterioscler Thromb Vasc Biol.* 2014;34:386-396. doi: 10.1161/ATVBAHA.113.302448
38. Kugo H, Moriyama T, Zaima N. Adipocytes and Abdominal Aortic Aneurysm: Putative Potential Role of Adipocytes in the Process of AAA Development. *Curr Drug Targets.* 2018;19:1228-1232. doi: 10.2174/1389450119666180115164103

7. Acknowledgments: None.

8. Sources of Funding

This work was supported by the National Natural Science Foundation of China (grants 82170507 and 81970402 to Jian Zhang, grant 81800407 to Han Jiang, grant 81600370 to Yanshuo Han), Liaoning Provincial Applied Basic Research Program (grant 2022JH2/101300037 to Jian Zhang), International Science and Technology Cooperation Program of Liaoning Province (grant: 2023JH2/10700019 to Han Jiang), the Natural Science Foundation of Liaoning Province (grant: 2023-MS-096 to Yanshuo Han).

9. Disclosures

Authors declare that they have no competing interests.

10. Legend of Tables

Table 1. MR results of PBMC eQTL for colocalized genes with AAA GWAS.

Table 2. MR results of Aorta eQTL for colocalized genes with AAA GWAS.

Table 3. The baseline data of AAA patients (n=7) and normal control group (n=3) included in this study for scRNA-seq.

11. Supplemental Material

Supplementary File – Table S1. Data types and sources for AAA PBMC samples.

Supplementary File – Table S2. The baseline data of AAA patients (n=20) and normal control group (n=10) from CMU aneurysm Biobank included in this study for proteomics and ATAC-seq.

Supplementary File – Table S3. The primer sequence of relative genes.

Supplementary File – Methods

Supplementary File – Excel 1. Summary-Level Mendelian Randomization (SMR) results for Aorta eQTL, PBMC eQTL, and whole blood mQTL with GWAS.

Supplementary File – Excel 2. Bayesian Colocalization Analysis using Bayes Factors (COLOC) results for Aorta eQTL and PBMC eQTL with GWAS.

Supplementary File – Excel 3. Results of confounder queries for the SNPs used as instrumental variables in MR, based on the GWAS Catalog.

Supplementary File – Excel 4. Pleiotropy test, heterogeneity test, direction

test, and Steiger test results for MR of PBMC eQTL for colocalized genes with AAA GWAS.

Supplementary File – Excel 5. Pleiotropy test, heterogeneity test, direction test, and Steiger test results for MR of Aorta eQTL for colocalized genes with AAA GWAS.

Supplementary File – Excel 6. Differential peaks analysis results from ATAC-seq for two AAA samples compared with a normal sample, respectively.

Supplementary File – Excel 7. Differential analysis results of single-cell data from AAA aorta tissue and PBMC, compared with their respective control groups across different cell types.

Supplementary File – Excel 8. Proteomic differential analysis results for two AAA samples compared with a normal sample, respectively.

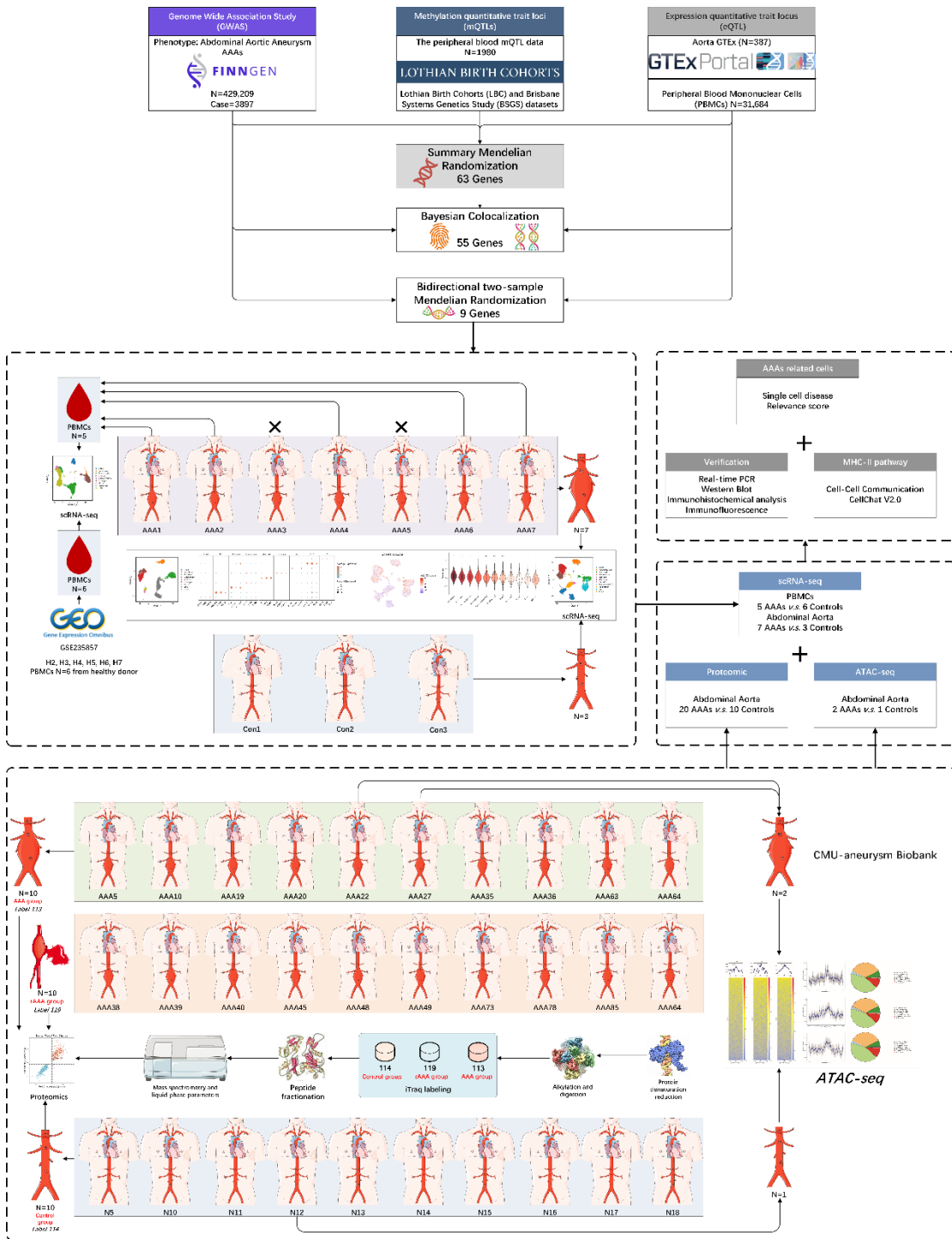


Figure 1. Flowchart of the overall experimental design.

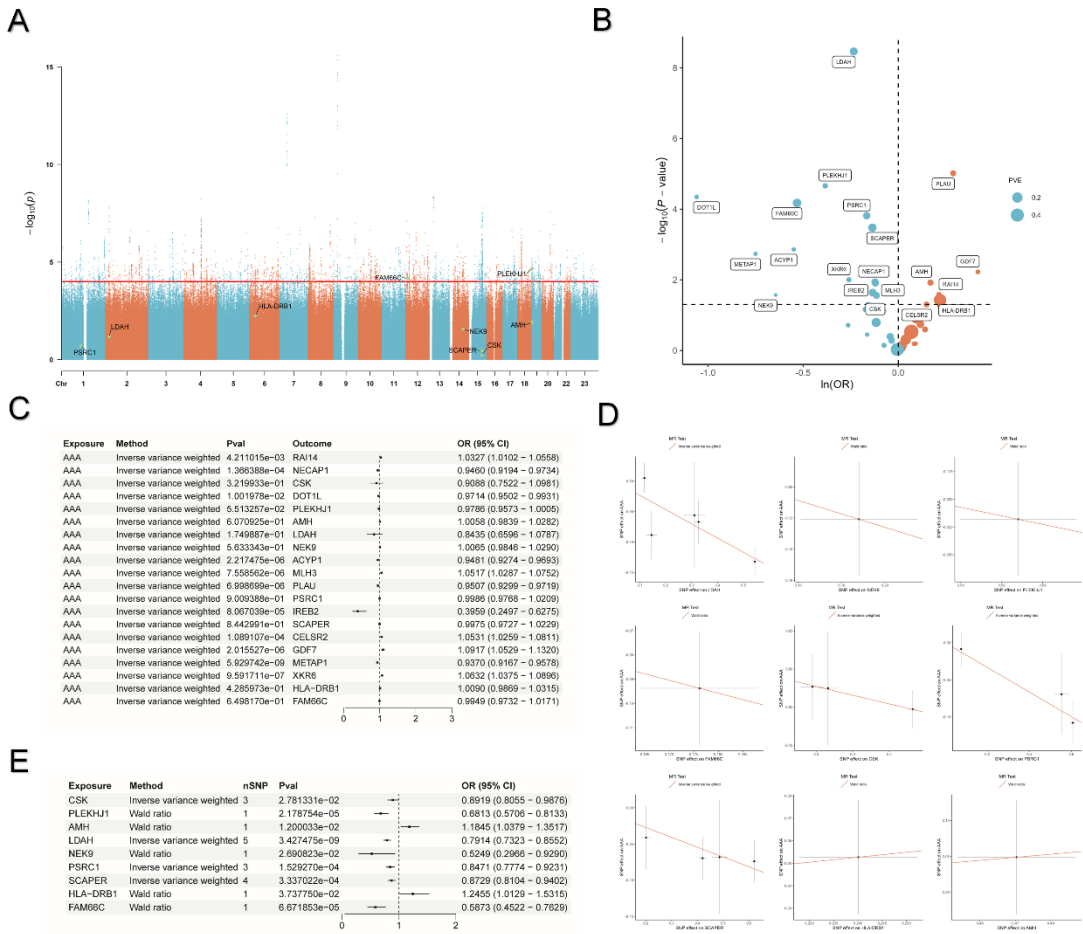


Figure 2. Genetic Analysis and Mendelian Randomization Results for Causal Genes in GWAS of Abdominal Aortic Aneurysm. (A) Manhattan plot of the AAA GWAS. The labels indicate the locations of the 9 causal genes identified in this study, with the y-axis representing the negative log of the p-value for one of the instrumental SNPs. (B) MR analysis results of colocalized genes. The teal points on the left side of the volcano plot represent genes with a negative OR, while the orange-red points on the right side indicate genes with an OR greater than zero. The y-axis shows the negative logarithm of the p-value, and the size of the points represents the proportion of variance explained (PVE). (C) Forest plot of reverse MR analysis results. (D) Forest plot of the 9 causal genes. (E) MR scatter plot for the 9 causal genes. In

cases where the number of instrumental SNPs is greater than 1, inverse variance weighted regression is used, and where the number is equal to 1, the Wald ratio estimate is applied.

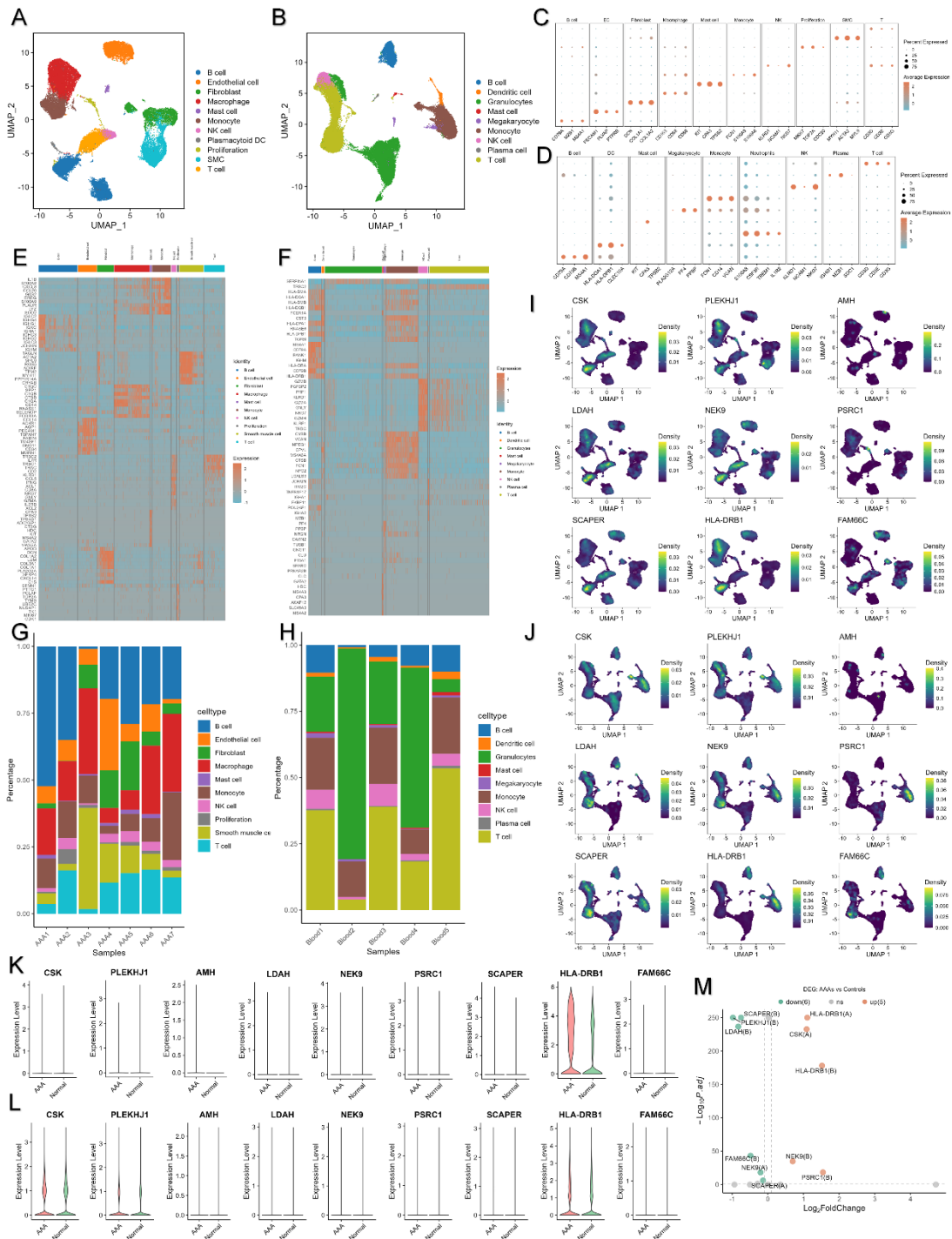


Figure 3. Cell Type Characterization and Expression Analysis of Causal Genes in AAA Tissue and PBMCs. UMAP plots of AAA tissue and PBMCs from AAA patients, respectively. (C-D) Dot plots displaying markers used to annotate cell types in AAA aortic tissue and PBMCs. (E-F) Heatmaps showing the expression profiles of the top genes in different cell types within aortic

tissue and PBMCs, respectively. (G) Bar plot of cell proportions across 7 AAA tissue samples. (H) Bar plot of cell proportions across 5 AAA PBMC samples. (I-J) Density plots of the expression distribution of 9 causal genes across different cell types in AAA tissue and PBMCs, respectively. (K) Expression levels of the 9 genes in AAA versus normal aortic tissue samples. (L) Expression levels of the 9 genes in AAA versus normal PBMC samples. (M) Differential expression analysis of the 9 genes in both tissue and PBMC samples overall. Teal color indicates lower expression relative to the control group, while orange-red indicates higher expression relative to the control group. Scatter points with the suffix 'A' represent differential expression in tissue, while those with the suffix 'B' represent differential expression in PBMCs.

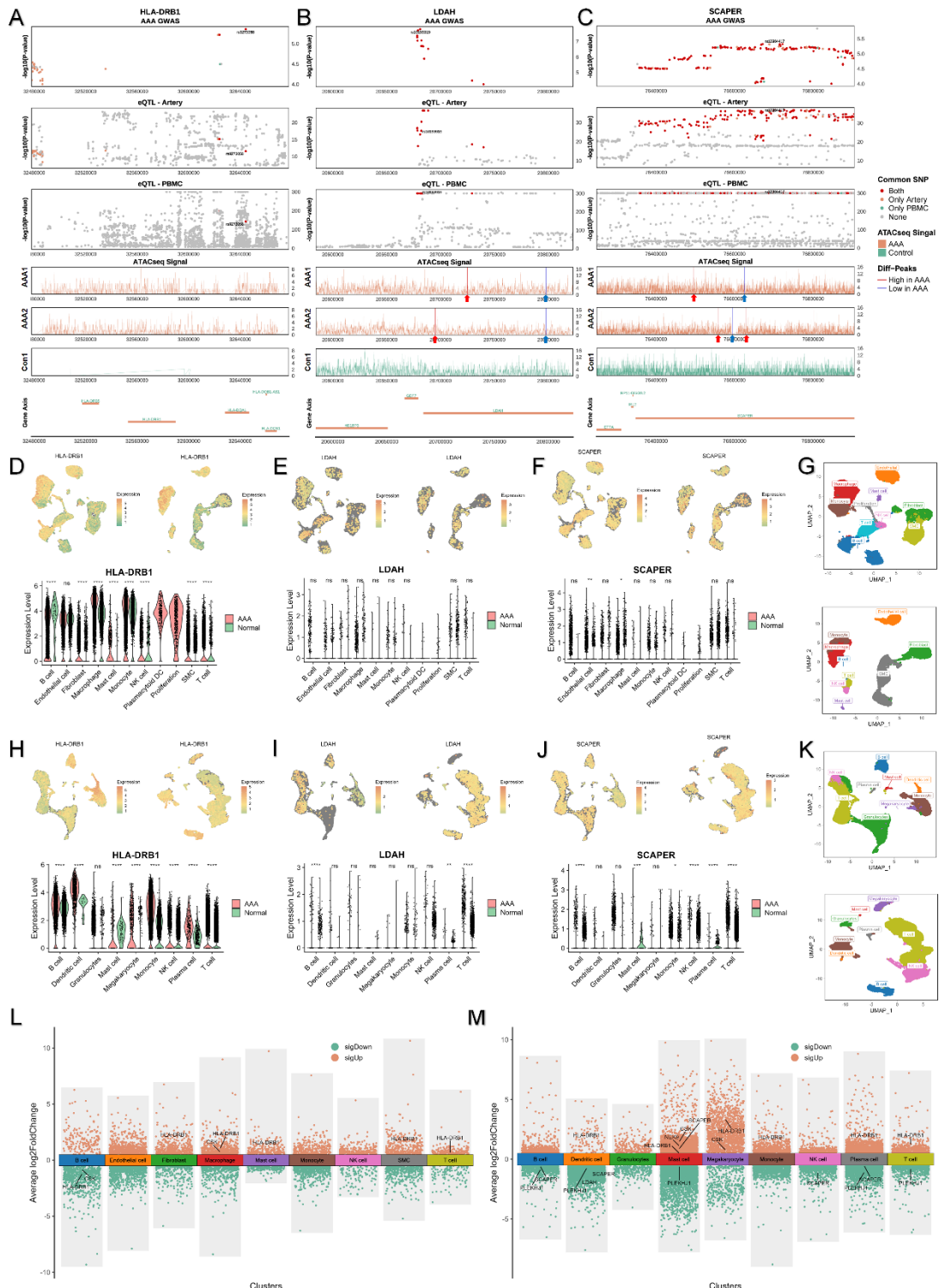


Figure 4. Colocalization and Expression Analysis of HLA-DRB1, LDAH, and SCAPER in AAA Tissue and PBMCs. Composite plots for HLA-DRB1, LDAH, and SCAPER gene regions depicting SNP colocalization and ATAC-seq signal levels. The first three panels within each composite plot

display SNP colocalization across AAA GWAS, aortic tissue eQTL (from GTEx), and PBMC eQTL. Each significant SNP within the region (GWAS threshold $P<1\times10^{-4}$, eQTL threshold $P<1\times10^{-8}$) is represented by a scatter point: red points indicate SNPs significantly colocalized in GWAS, aortic tissue eQTL, and PBMC eQTL simultaneously; orange-red points represent SNPs colocalized only in aortic tissue; blue points indicate SNPs colocalized only in PBMC; and gray points represent SNPs that are not colocalized. The three-line graphs depict ATAC-seq signal values, with regions marked by blue arrows and vertical lines indicating downregulated differential peaks in AAA, and red marks indicating upregulated peaks. The gene tracks for the region are shown at the bottom of each composite plot. (D-F) Expression profiles of HLA-DRB1, LDAH, and SCAPER in aortic tissue. The feature plots on the left are from AAA tissue, while those on the right are from normal aortic tissue. The violin plots below show the expression levels and differences (Wilcoxon test) of these genes across different cell types. (G) UMAP plots of cells within AAA and normal aortic tissue, used to compare cell types. (H-J) Expression profiles of the three genes in PBMCs. (K) UMAP plot of PBMCs. (L, M) Differential expression analysis in AAA tissue and PBMCs, showing genes with $|Log2(Fold Change)| > 0.5$ in each cell type. * $P<0.05$, ** $P<0.01$, *** $P<0.001$, **** $P<0.0001$

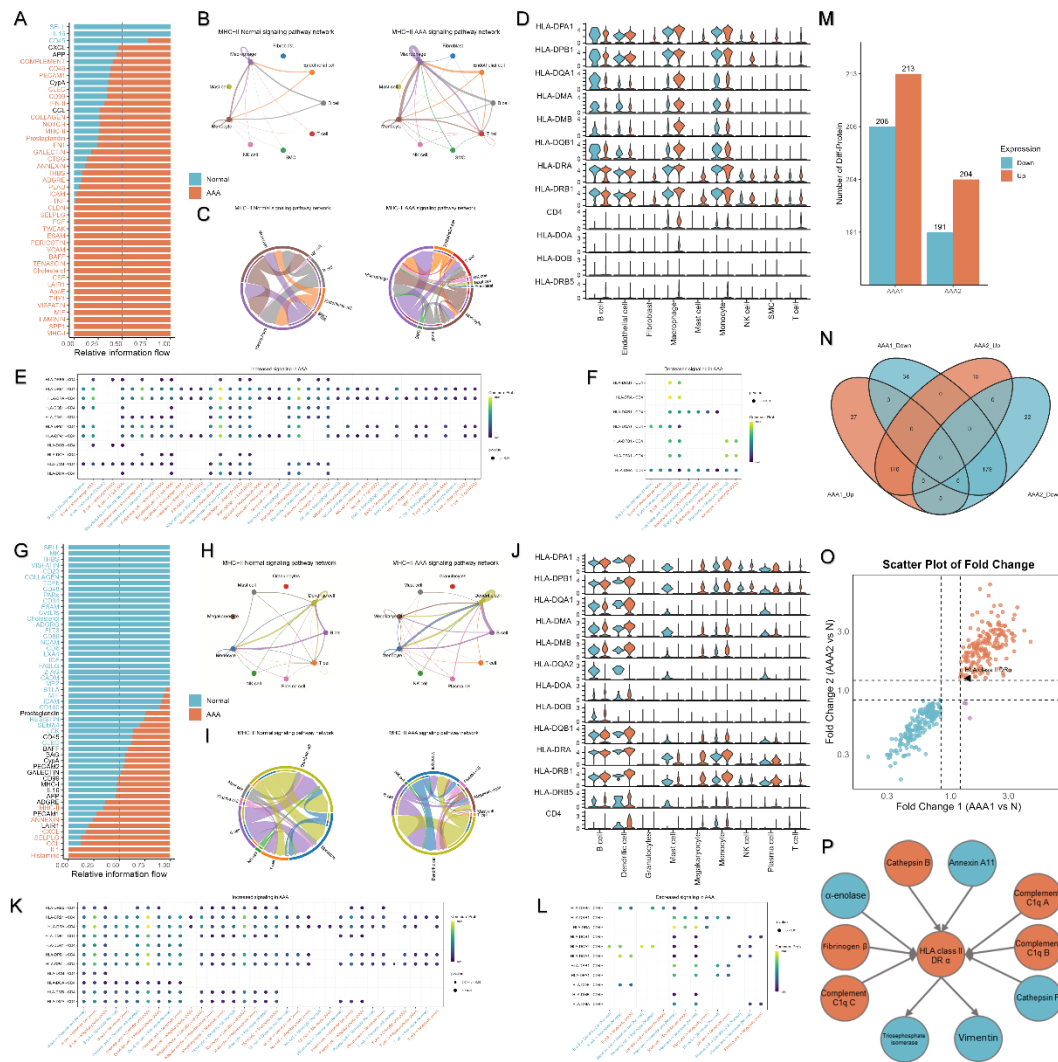


Figure 5. Differential Pathways of Cell-Cell Communication and MHC-II Signaling in AAA Aortic Tissue and PBMCs.

(A) Differential pathways of cell-cell communication in aortic tissue. The x-axis represents the relative information flow between the AAA and normal groups, with orange-red indicating upregulation in AAA and teal indicating downregulation in AAA. (B) Network diagram of MHC-II signaling pathways between cells, where the width of the connections represents the strength of communication. (C) Chord diagram showing the relative strength of MHC-II signaling pathways between cells. (D) Violin plots displaying the expression levels and differences of MHC-II signaling-related genes across different cell types in aortic tissue, blue

represents normal samples, while red indicates samples associated with AAA. (E, F) Upregulated and downregulated signals in AAA aortic tissue, respectively. The closer the color of the dots is yellow, the higher the probability value and communication level. (G-L) Intercellular communication of the MHC-II pathway in AAA PBMCs and the differences compared to the control group, similar to the content shown in the aortic tissue plots. (M) Bar chart showing the number of differentially expressed proteins in the proteomics analysis. (N) Venn diagram illustrating the intersection of differentially expressed proteins in two replicates. (O) Scatter plot showing genes that were differentially expressed in both replicates, with the x and y axes representing fold change (FC > 1.2 considered significant). Orange-red dots represent proteins that were upregulated in both replicates, while teal dots represent proteins that were downregulated in both. (P) Interaction network of differentially expressed proteins interacting with HLA class II DR α protein, with orange-red indicating proteins upregulated in both replicates and teal indicating proteins downregulated in both.

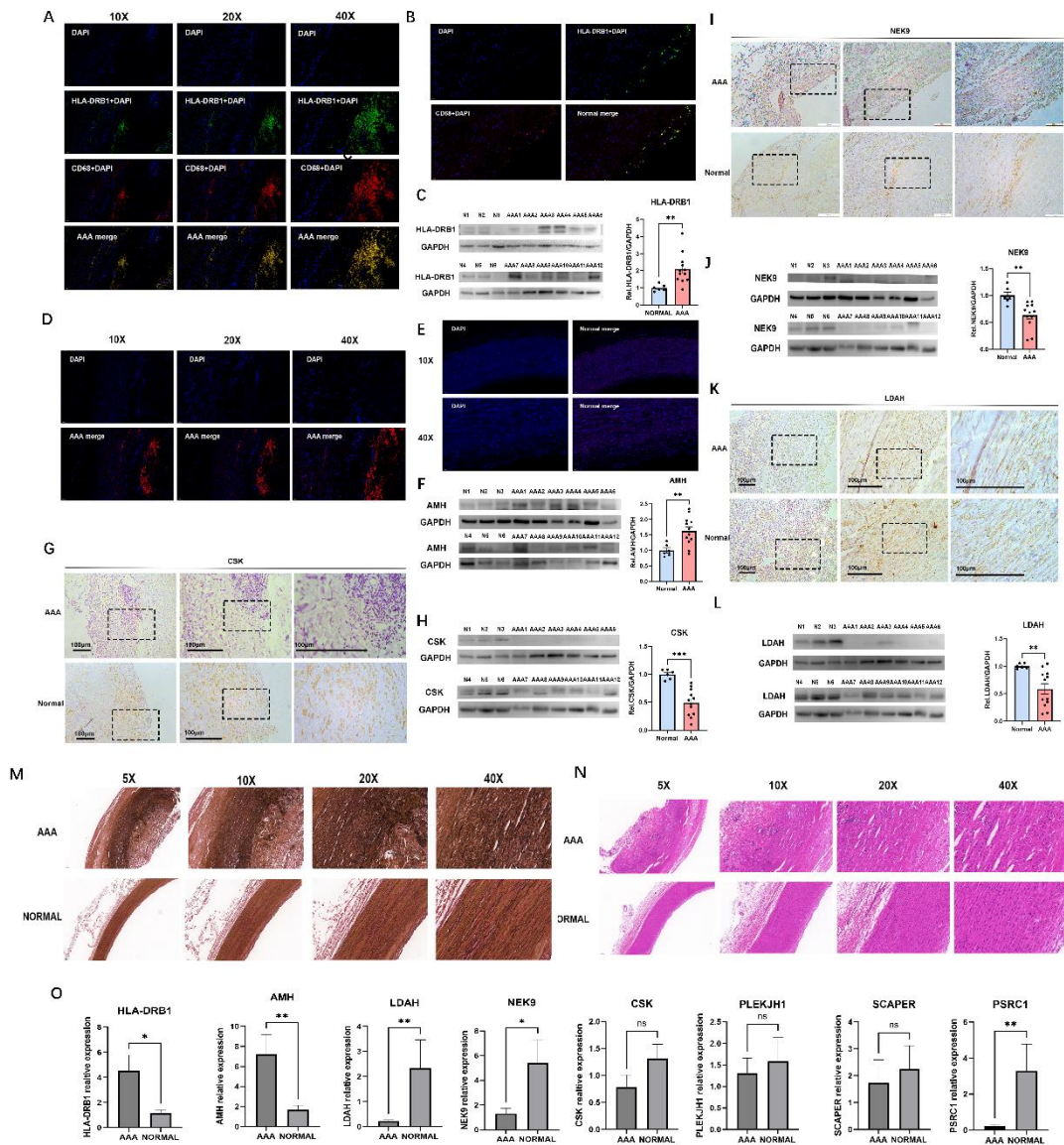
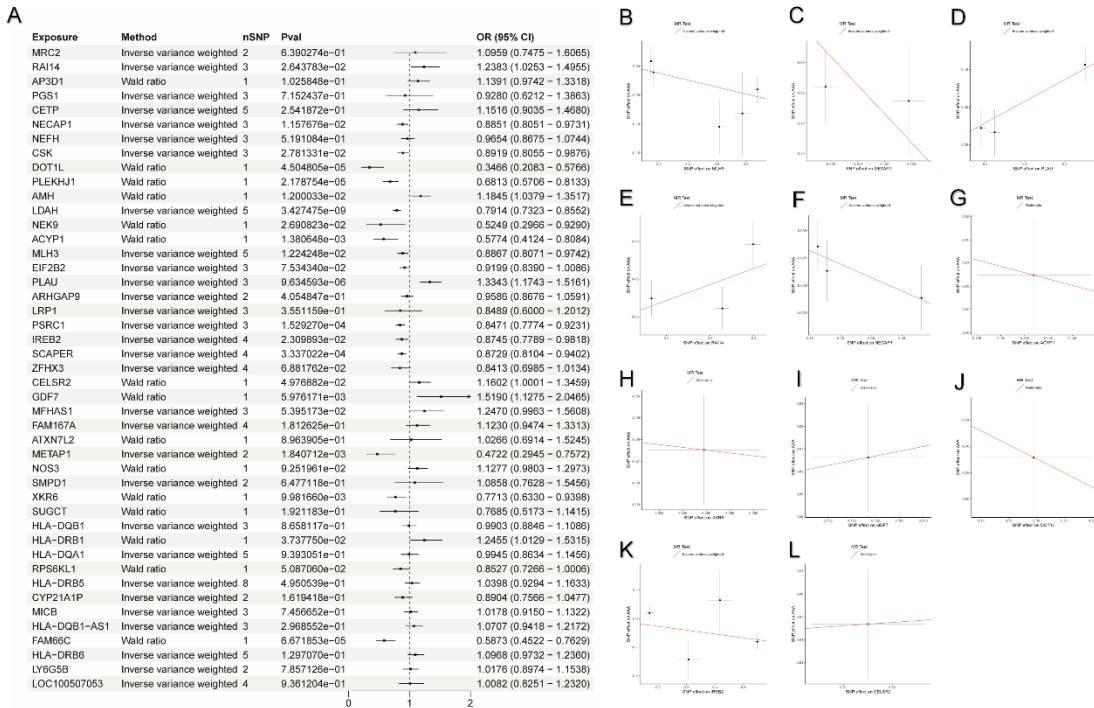
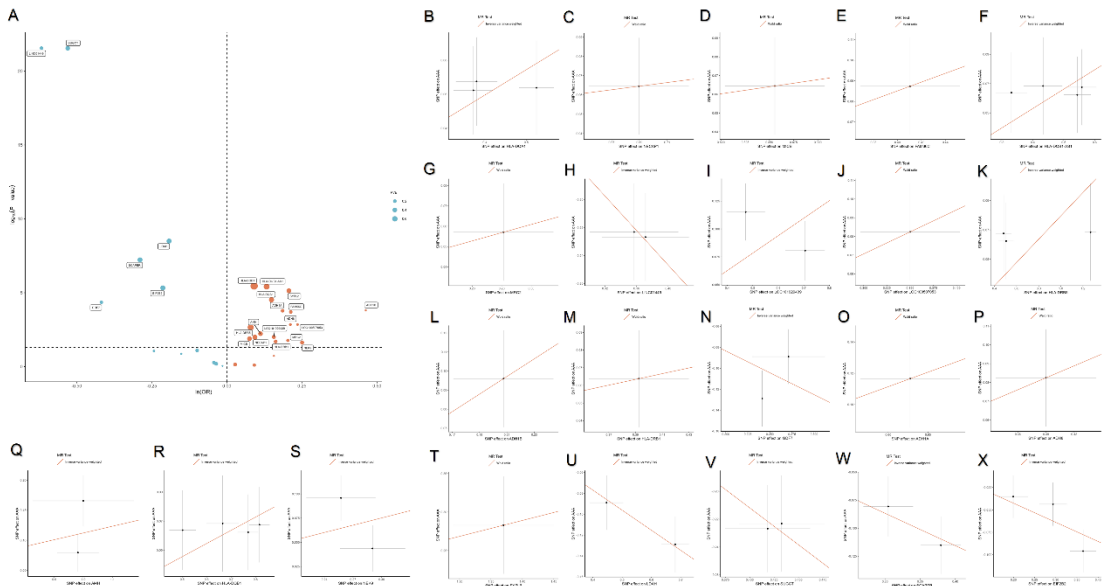


Figure 6. Immunofluorescence and Expression Analysis of HLA-DRB1, AMH, CSK, NEK9, and LDAH in Human AAA Tissue. IF staining results of human AAA samples at different magnifications (10X, 20X, 40X). The blue regions represent cell nuclei stained with DAPI, while green and red indicate the specific expression of HLA-DRB1 and the macrophage marker CD68, respectively. The overlapping areas suggest interactions between macrophages and HLA-DRB1 in human AAAs (A); Co-localization of CD68 and HLA-DRB1 in normal human samples (B); Western blot analysis showing

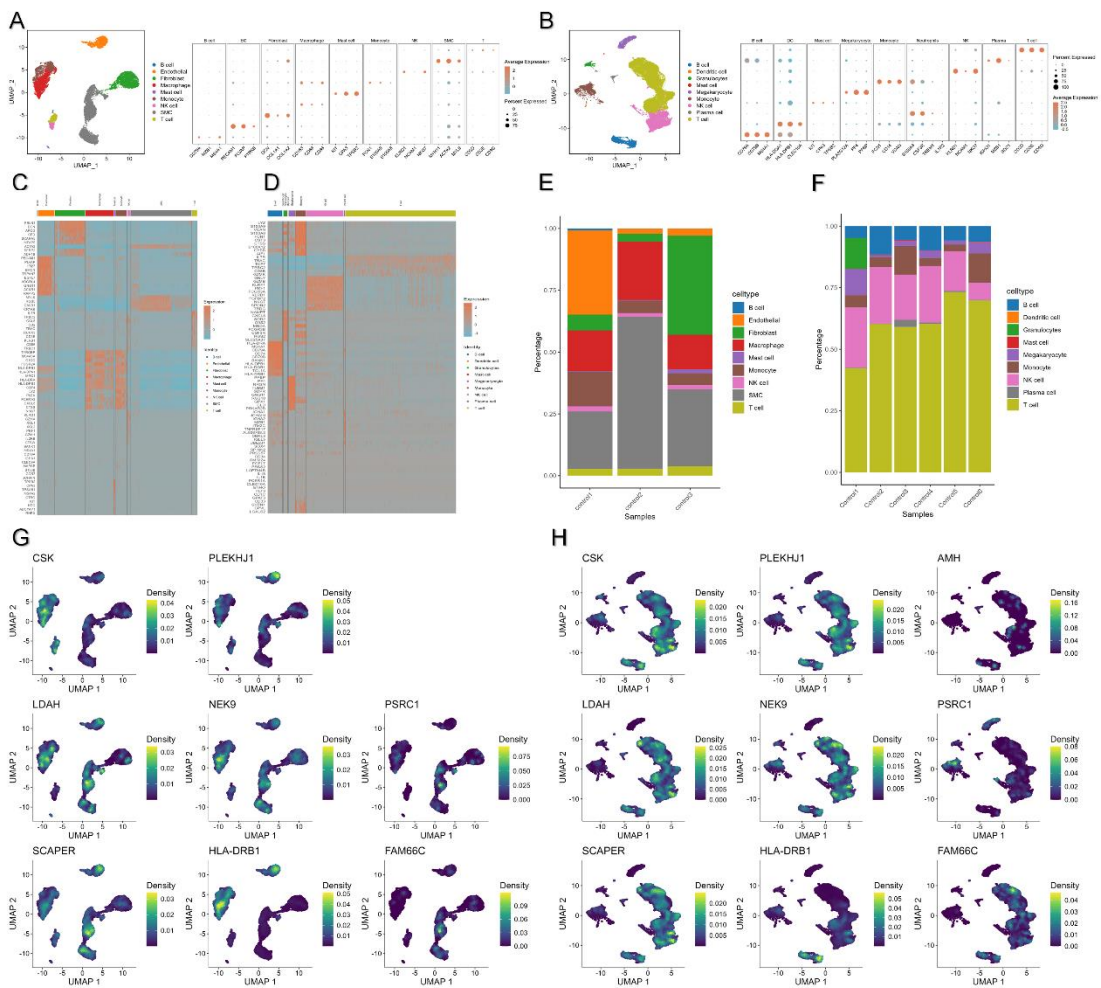
the expression of HLA-DRB1 in AAA and normal tissues (C); IF staining results of human AAA samples at different magnifications (10X, 20X, 40X), with red fluorescence representing the target gene AMH (D). DAPI (blue) and target gene ²¹ staining of normal human samples at 10X and 40X magnification (E); Western blot analysis showing the expression of AMH in AAA and normal tissues (F); Immunohistochemistry (IHC) staining of CSK, scale bar = 100 µm (G); CSK protein expression in AAA and normal tissues (H); IHC staining of NEK9, scale bar = 100 µm (I); NEK9 protein expression in AAA and normal tissues (J); IHC staining of LDAH, scale bar = 100 µm(K); LDAH expression in AAA and normal tissues (L); Histological staining results of EVG between AAA and NORMAL (M); HE staining results between abdominal aortic aneurysm and normal tissue(N) qPCR results of aortic tissues from AAA patients and normal individuals, measured using the $2^{(-\Delta\Delta CT)}$ method to determine relative expression levels (O). Data are presented as mean \pm SEM, (Normal n = 6 and AAA n = 12). DAPI represents 4',6-diamidino-2-phenylindole. Representative images of immunofluorescence staining. *P < 0.05, **P < 0.01, ***P < 0.001, ****P < 0.0001



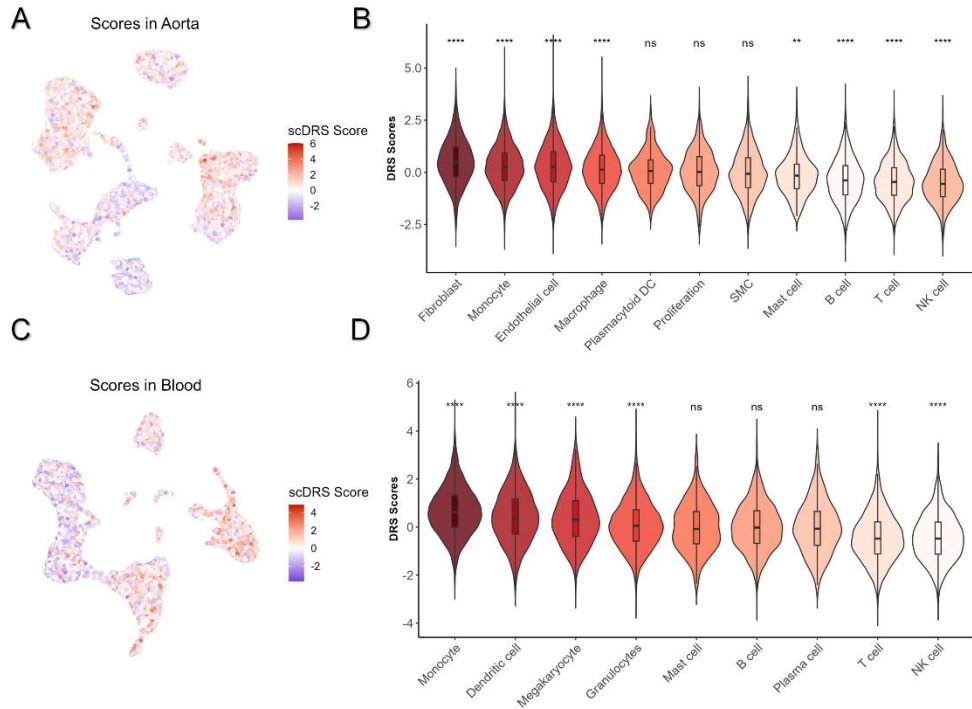
Supplementary Figure 1 (A) Forest plot of MR results for all colocalized genes. (B) Scatter plot of MR test results for genes with p-values less than 0.05 in both forward and reverse MR analyses. The Inverse Variance Weighted (IVW) method was used when the number of instrumental SNPs was greater than one, and the Wald ratio was used when the number was equal to one.



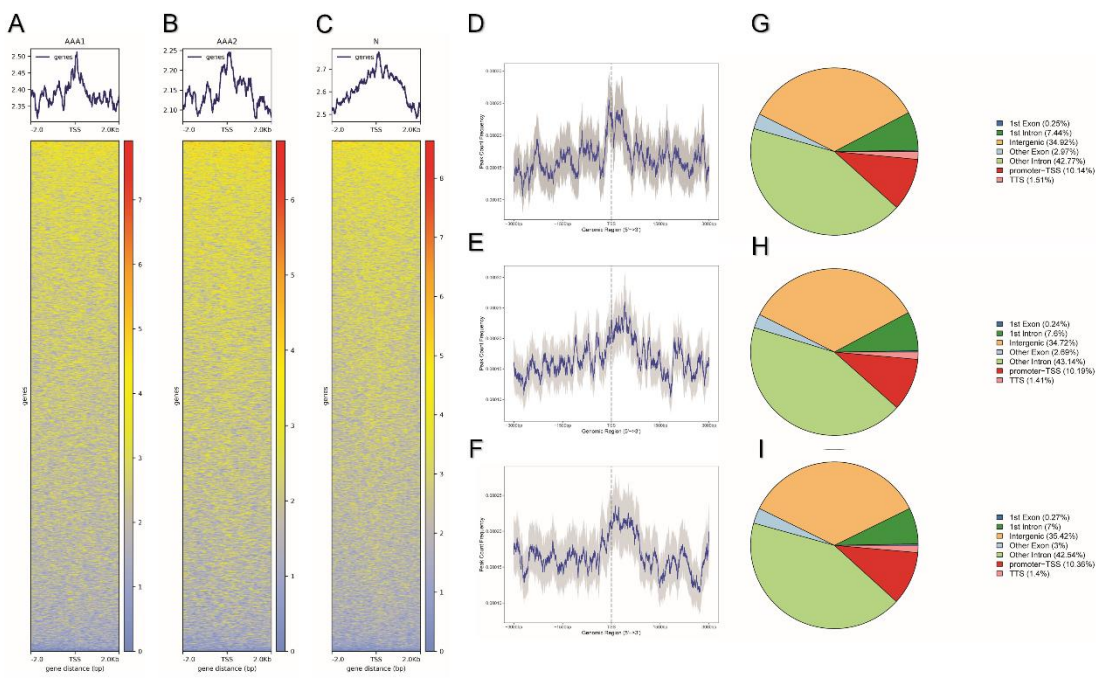
Supplementary Figure 2 (A) This volcano plot shows the MR analysis results using Aorta eQTL data and AAA GWAS. Blue-green dots on the left represent genes with negative OR values, while orange-red dots on the right represent genes with positive OR values. The y-axis represents the negative logarithm of the p-value, and the size of the dots represents the proportion of variance explained (PVE). (B) Scatter plot of MR test results for the 23 genes with p-values less than 0.05 (using Aorta eQTL data). The IVW method was used when the number of instrumental SNPs was greater than one, and the Wald ratio was used when the number was equal to one.



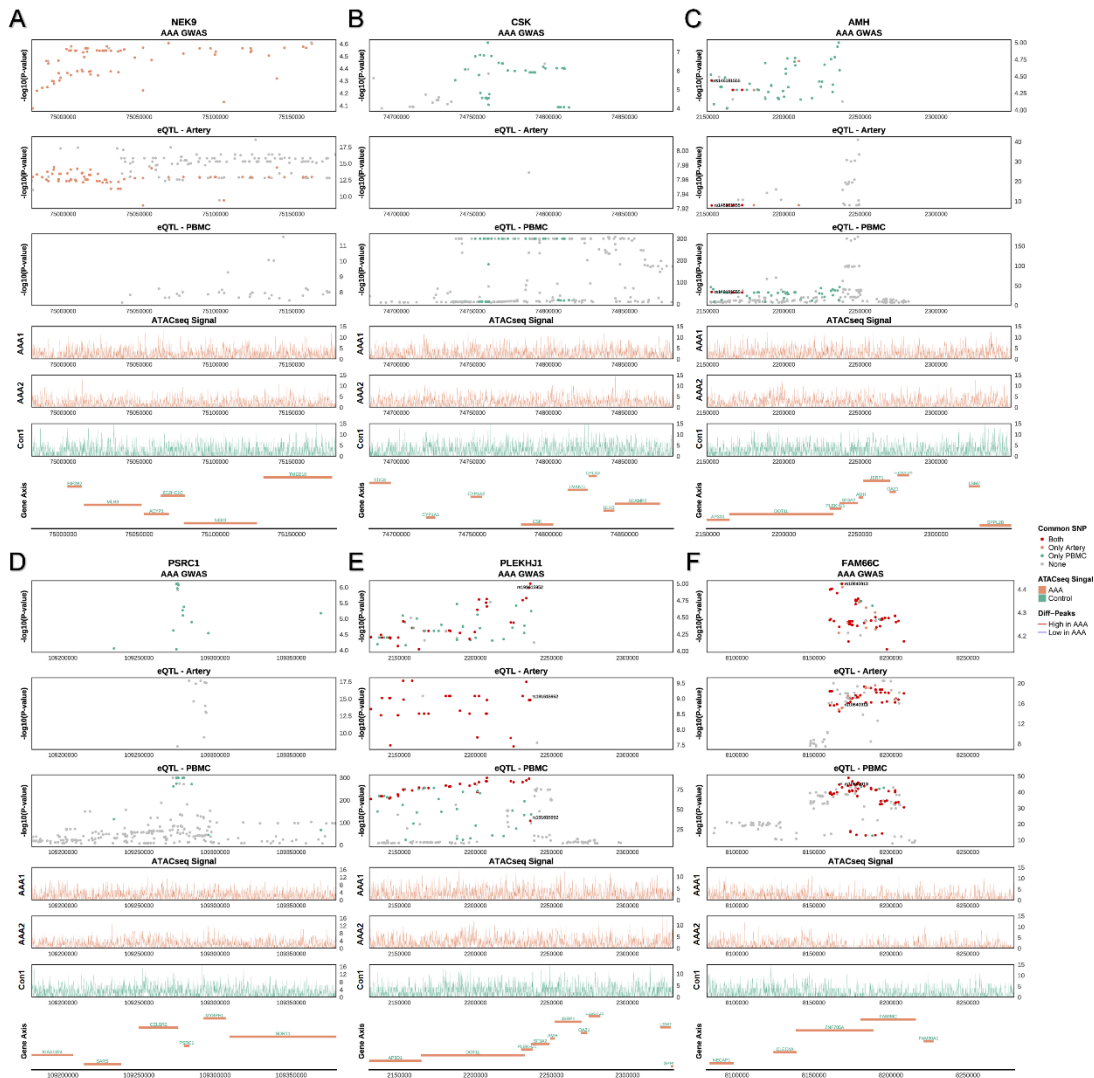
Supplementary Figure 3 (A-B) UMAP plot and dot plot of marker genes for annotated single-cell data from normal aorta tissue and PBMC. (C-D) Heatmaps showing the top genes in various cell types of normal aorta and PBMC. (E-F) Bar plots showing the proportions of normal samples in aorta and PBMC. (G-H) Density distribution plots of nine causal effect genes in normal samples.



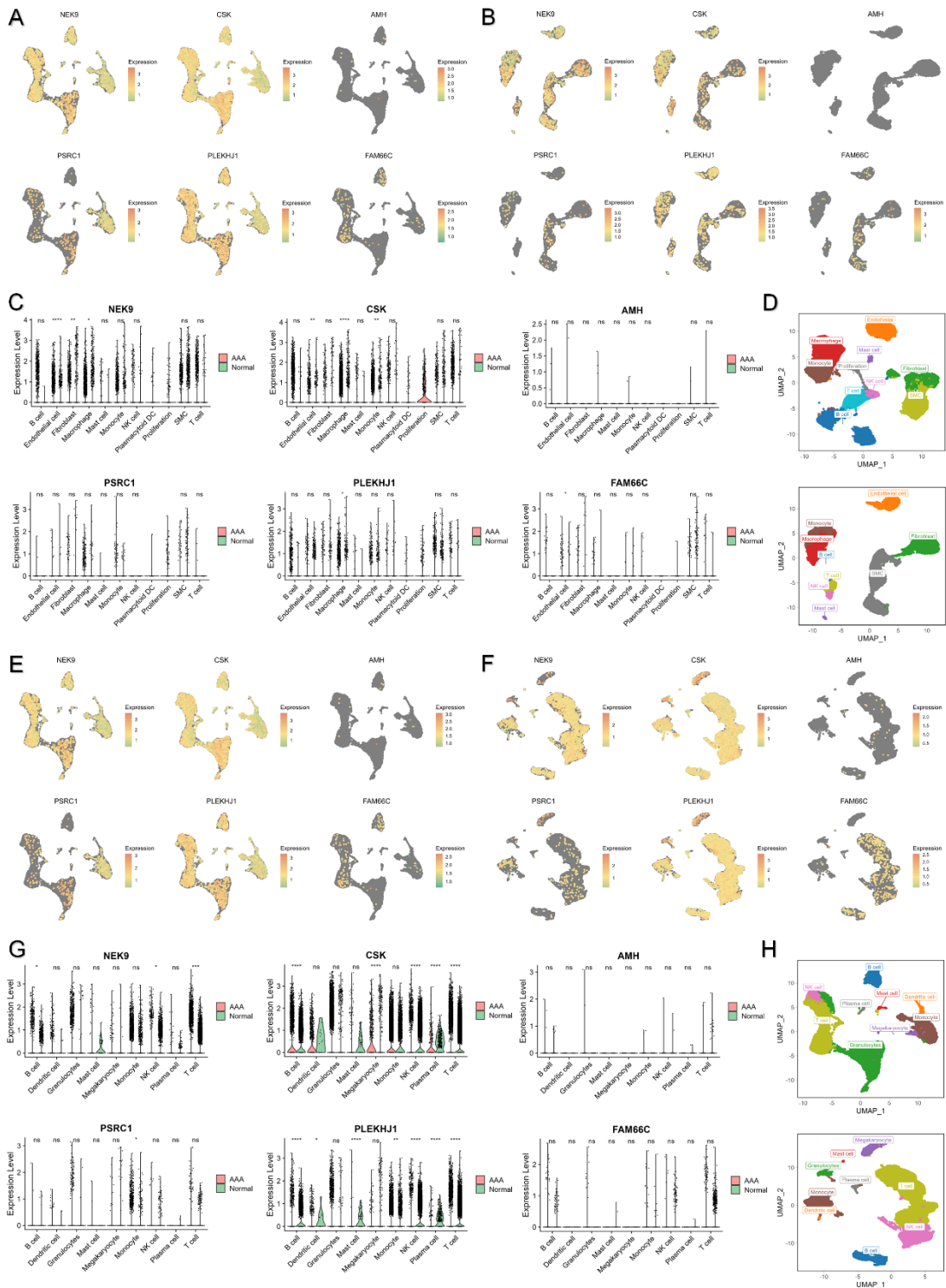
Supplementary Figure 4 (A) Feature plot of scDRS scores in AAA aorta tissue. (B) Violin plot of scDRS scores in various cell types in AAA tissue, with significance levels marked based on Wilcoxon test comparisons against the mean of other cells. (C) Feature plot of scDRS scores in AAA PBMC. (D) Violin plot of scDRS scores in various cell types in AAA PBMC. (* $P<0.05$, ** $P<0.01$, *** $P<0.001$, **** $P<0.0001$)



Supplementary Figure 5 (A-C) Distribution of ATAC-seq peaks around transcription start sites (TSS) in two AAA samples and one normal sample. (D-F) Frequency distribution around TSS in the three samples. (G-I) Proportional annotation of differential peaks in the three samples.

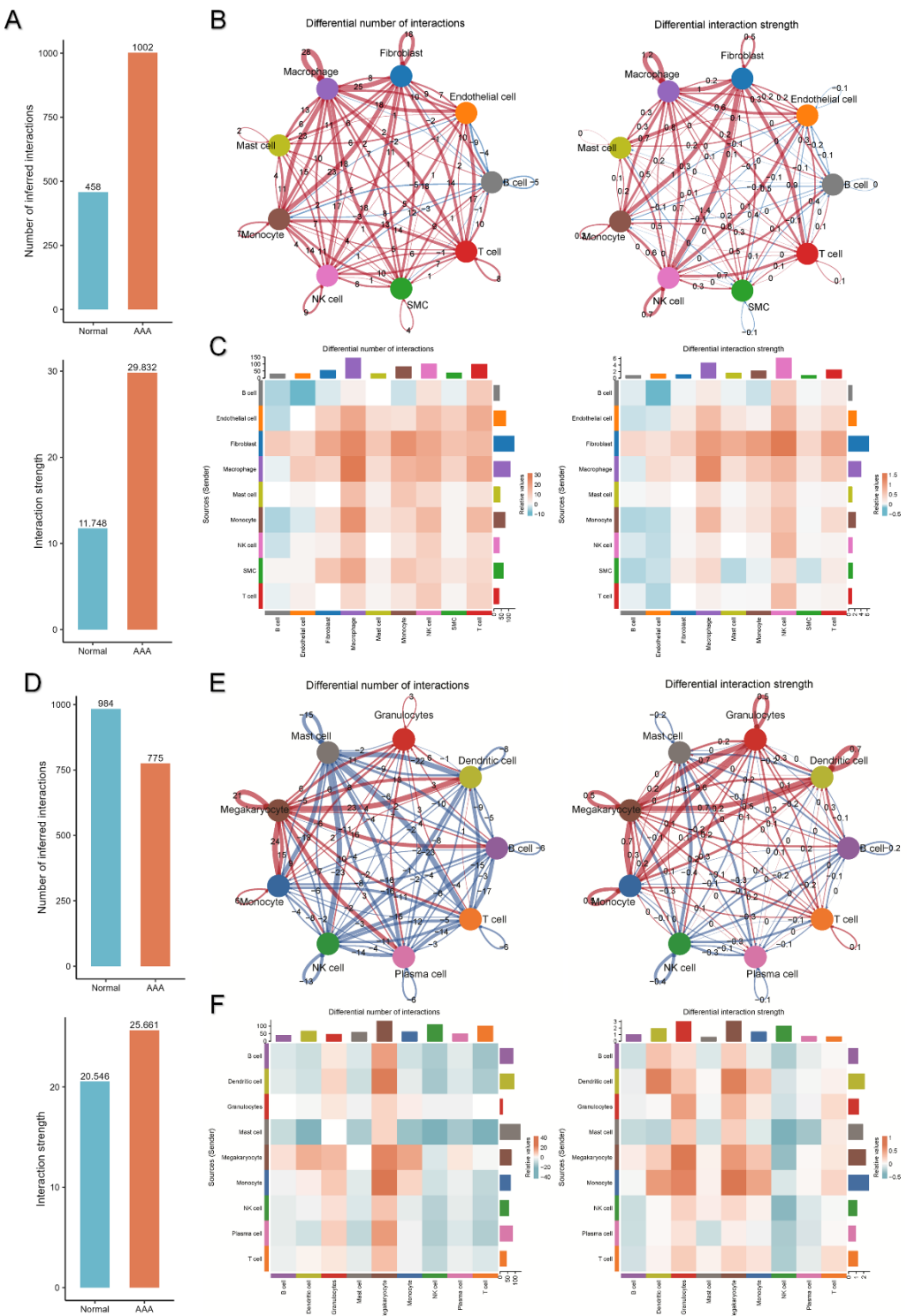


Supplementary Figure 6 Composite figure showing colocalization and ATAC-seq signal values for the remaining six causal effect genes (NEK9, CSK, AMH, PSRC1, PLEKHJ1, FAM66C). No differential peaks were detected for these genes.



Supplementary Figure 7 (A) Feature plots of the remaining six causal genes (NEK9, CSK, AMH, PSRC1, PLEKHJ1, FAM66C) in AAA aorta tissue. **(B)** Feature plots of the remaining six causal genes in normal aorta tissue. **(C)** Violin plots showing expression differences of the six genes in different cell types in the aorta, with AAA on the left and

normal on the right. (E-H) Single-cell expression maps of the six genes in PBMC, displayed in the same manner as in the aorta. (* $P<0.05$, ** $P<0.01$, *** $P<0.001$, **** $P<0.0001$)



Supplementary Figure 8 (A) Bar plots showing the number and strength of cell communications in the entire AAA aorta, with the upper and lower bars representing different metrics. (B) Network diagram of cell communications in AAA aorta tissue, with red lines indicating stronger communication levels in AAA compared to normal,

and blue lines indicating the opposite. The numbers in the diagram represent the differences in the number and strength of communications between AAA and normal.

(C) Heatmap of communication differences, with orange-red indicating upregulation in AAA and blue-green indicating downregulation. The left side of the heatmap shows the signal senders, and the bottom shows the signal-receiving cell types. (D-F) Overview of cell communication in PBMC, with similar visualizations as in panels A-C.